Redox Biology 60 (2023) 102618

Contents lists available at ScienceDirect

Redox Biology

journal homepage: www.elsevier.com/locate/redox

FUT2-dependent fucosylation of HYOU1 protects intestinal stem cells against inflammatory injury by regulating unfolded protein response

Zhe Wang [1], Chen Tan [1], Caihan Duan, Junhao Wu, Dan Zhou, Lingzhi Hou, Wei Qian, Chaoqun Han [*], Xiaohua Hou [**]

Division of Gastroenterology, Union Hospital, Tongji Medical College, Huazhong University of Science and Technology, Wuhan, 430022, China

ARTICLE INFO

Keywords:
FUT2
Fucosylation
Intestinal stem cell
Inflammatory injury
Apoptotsis
Unfolded protein response

ABSTRACT

The intestinal epithelial repair after injury is coordinated by intestinal stem cells (ISCs). Fucosylation catalyzed by fucosyltransferase 2 (FUT2) of the intestinal epithelium is beneficial to mucosal healing but poorly defined is the influence on ISCs. The dextran sulfate sodium (DSS) and lipopolysaccharide (LPS) model were used to assess the role of FUT2 on ISCs after injury. The apoptosis, function, and stemness of ISCs were analyzed using intestinal organoids from WT and *Fut2*$^{\Delta ISC}$ (ISC-specific *Fut2* knockout) mice incubated with LPS and fucose. *N*-glycoproteomics, UEA-1 chromatography, and site-directed mutagenesis were monitored to dissect the regulatory mechanism, identify the target fucosylated protein and the corresponding modification site. Fucose could alleviate intestinal epithelial damage via upregulating FUT2 and α-1,2-fucosylation of ISCs. Oxidative stress, mitochondrial dysfunction, and cell apoptosis were impeded by fucose. Meanwhile, fucose sustained the growth and proliferation capacity of intestinal organoids treated with LPS. Contrarily, FUT2 depletion in ISCs aggravated the epithelial damage and disrupted the growth and proliferation capacity of ISCs via escalating LPS-induced endoplasmic reticulum (ER) stress and initiating the IRE1/TRAF2/ASK1/JNK branch of unfolded protein response (UPR). Fucosylation of the chaperone protein HYOU1 at the *N*-glycosylation site of asparagine (Asn) 862 mediated by FUT2 was identified to facilitate ISCs survival and self-renewal, and improve ISCs resistance to ER stress and inflammatory injury. Our study highlights a fucosylation-dependent protective mechanism of ISCs against inflammation, which may provide a fascinating strategy for treating intestinal injury disorders.

1. Introduction

The intestinal mucosal barrier is the first line of defense to prevent harmful substances such as intestinal bacteria and toxins from entering the body [1]. Breakdown of the intestinal barrier and impaired epithelial repair have been linked to the pathogenesis of a series of gastrointestinal and systemic diseases including inflammatory bowel disease (IBD), acute pancreatitis, and many other critical diseases [2–4]. Epithelial repair is critical for barrier function maintenance after intestinal injury, but there are few measures to facilitate epithelial repair after injury in clinical practice [5]. Current strategies which mainly focus on the interruption of inflammatory progression for intestinal epithelial disorders like IBD can hardly achieve complete mucosal healing [6]. On these grounds, strategies pursued complete regeneration of the intestinal mucosal demand prompt solutions [7,8].

In the intestinal epithelium, the homeostatic constant regeneration and self-renewal are driven by Lgr5^{+} intestinal stem cells (ISCs) that reside at the base of epithelial crypts [9,10]. In response to various injury, ISCs increase their proliferation rates and differentiate into multiple epithelial cell types to replenish the damaged cells for mucosal healing [11,12]. While excessive pathogenic factors can induce the constant depletion of ISCs and the disrupted balance of stem cell fate [13]. Therefore, a better understanding of facilitating stemness maintenance and stress resistance to oxidative stress and apoptosis of ISCs to fulfill complete regeneration is demand for complete mucosal healing.

Control of quantity and stemness of ISCs is essential for tissue homeostasis [14]. Various disturbances of intestinal homeostasis including

* Corresponding author. Division of Gastroenterology, Union Hospital, Tongji Medical College, Huazhong University of Science and Technology, 1277 Jiefang Avenue, Wuhan, Hubei Province, 430022, China.

** Corresponding author. Division of Gastroenterology, Union Hospital of Tongji Medical College, Huazhong University of Science and Technology, 1277 Jiefang Avenue, Wuhan, Hubei Province, 430022, China.

E-mail addresses: hcq1987912@hotmail.com (C. Han), houxh@hust.edu.cn (X. Hou).

[1] These authors contributed equally to this work.

https://doi.org/10.1016/j.redox.2023.102618
Received 8 December 2022; Received in revised form 16 January 2023; Accepted 24 January 2023
Available online 28 January 2023

Abbreviations

ATF6	transcription factor 6
DAI	disease activity index
DSS	dextran sulfate sodium
ER	endoplasmic reticulum
FACS	fluorescence activated cell sorting
FUC	Fucose
FUT2	fucosyltransferase 2
Fut2$^{\Delta ISC}$	*Fut2* gene specifically deleted in intestinal stem cell
GFP	green fluorescent protein
GO	gene ontology
IBD	inflammatory bowel disease
IRE1	inositol-requiring kinase 1
ISC	intestinal stem cell
LPS	lipopolysaccharide
MMP	mitochondrial membrane potential
PERK	protein kinase RNA-like ER kinase
ROS	reactive oxygen species
UEA-1	ulex europaeus agglutinin-1
UPR	unfolded protein response
WT	wild type

inflammation stimuli, oxidative stress, metabolic alterations, and defective glycosylation can alter cellular protein homeostasis and trigger endoplasmic reticulum (ER) stress [15,16]. In response to ER stress, the unfolded protein response (UPR), an evolutionarily conserved adaptive mechanism caused by accumulation of unfolded or misfolded proteins, serves as the quality control pathway within the ISCs to decrease the burden of ER and restore stemness and tissue homeostasis [17,18]. Alternatively, irremediable ER stress leads to the activation of the pro-apoptotic UPR signaling to hasten cell demise [19]. Moreover, recent studies have revealed the role of UPR in control of the proliferative and regenerative capacities of ISCs, thus orchestrating epithelial regeneration response [20,21]. The UPR has evolved a complex network of interconnected signaling branches initiated by the recruitment of the ER chaperone glucose-regulated protein 78 (GRP78) [22,23] and the stimulation of three signal transducers known as inositol-requiring kinase 1 (IRE1), transcription factor 6 (ATF6), and protein kinase RNA-like ER kinase (PERK) [24,25]. Determining the function and fate of ISCs, UPR constitutes an attractive target for future therapeutic approaches to intestinal regeneration.

Fucose, a natural saccharide discovered in a variety of foods, has been reported in our previous studies and others to ameliorate intestinal inflammation and barrier dysfunction by upregulating fucosyltransferase 2 (FUT2) [26–28]. FUT2, a prominent enzyme responsible for the linkage of fucose to proteins or lipids by α-1,2-fucosylation, has been proven to be associated with chronic inflammatory diseases such as IBD [29,30]. The aberrant expression of FUT2 was both observed in the intestinal epithelium of patients with IBD and DSS-treated mice [31]. Moreover, fucosylation deficiency in mice led to colitis characterized by impaired mucosal integrity and aberrant crypts proliferation [32], which implied the potential role of fucosylation on tuning ISC fate. However, the effect and mechanism of fucose and FUT2-dependent fucosylation on ISCs remain unrevealed.

In this study, we aimed to investigate the protective effects of FUT2-dependent fucosylation on the ISC homeostasis and intestinal epithelial regeneration. ISC-specific *Fut2* knockout (*Fut2*$^{\Delta ISC}$) mice and organoid cultures were constructed to evaluate the crucial role of FUT2 in ISCs and the underlying regulatory mechanism upon inflammatory injury. The initiation of UPR and the target fucosylated protein were determined based on the data from the *N*-glycoproteomics of ISCs derived from WT and *Fut2*$^{\Delta ISC}$ mice. This study elucidated the significance of FUT2-dependent fucosylation on stem cell fate control and epithelial regeneration upon injury, which may throw novel insights into stem cell-based regenerative therapies for intestinal mucosal injury.

2. Materials and methods

2.1. Animal experiment

Lgr5-eGFP-IRES-Cre^{ERT2} mice (*Lgr5-Tg* mice) were bred with mice carrying floxed alleles for the *Fut2* gene (*Fut2*$^{flox/flox}$ C57BL/6 mice, purchased from GemPharmatech Co. Ltd) to generate the *Lgr5-eGFP-IRES-Cre*^{ERT2}*/Fut2*$^{fl/fl}$ mice (*Lgr5-Tg/Fut2*$^{fl/fl}$). Then tamoxifen was used to induce deletion of *Fut2* in *Lgr5*$^{+}$ cells (*Fut2*$^{ISC-/-}$ mice, abbreviated as *Fut2*$^{\Delta ISC}$), whereas *Lgr5-Tg* mice were used as control (abbreviated as WT). For *Fut2* deletion induction, male mice of 8- to 12-week-old were given 2 mg of tamoxifen (intraperitoneal injection; Sigma-Aldrich, T5648) for 5 consecutive days to ensure recombination in Lgr5^{+} cells. The efficacy of tamoxifen for *Fut2* deletion in ISC was validated by the immunofluorescence of green fluorescent protein (GFP), the down-regulation of FUT2 and the deficiency of α-1,2-fucosylation in the intestinal organoids. All mice were housed in the specific pathogen free (SPF) grade facility of Huazhong University of Science and Technology and maintained at 12 h light/dark cycles with free access to food and water. All animal experiments were carried out following the protocols approved by the Animal Experimentation Committee of Huazhong University of Science and Technology (IACUC No. S2529) and performed in accordance with national and EU guidelines.

2.2. Establishment of DSS model

Wild-type mice were randomly divided into four groups: control, fucose, dextran sulfate sodium (DSS; MW 36,000–50,000 Da; MP Biomedicals), and DSS + fucose groups (simplified as CON, FUC, DSS, and DSS + FUC) as privously described [27]. Acute intestinal injury was induced by administration of 3% (w/v) DSS in drinking water for 7 days and then followed by 3 days with normal drinking water. Fucose (250 mg/kg; Sigma-Aldrich, F2252), dissolved in saline, was given to mice by oral gavage once a day for 10 days. In the CON and DSS groups, the same volume of saline was given as vehicle control. Mice were sacrificed 4 days after DSS treatment. Tissues were collected for subsequent analysis.

During the course of the experiment, the body weight, stool consistency and bleeding were measured every day to assess the disease activity index (DAI) [33]. Briefly, DAI scores were defined as follows, for weight loss, 0: no loss; 1: 1–5% loss; 2: 5–10% loss; 3: 10–20% loss and 4: >20% weight loss; for stool consistency, 0: normal; 2: loose stool; 4: diarrhea; and for stool bleeding, 0: no blood; 2: presence and 4: gross blood.

2.3. Tissue immunostaining

For immunohistochemistry assays, intestinal tissue sections were dewaxed, rehydration and conducted antigen heat retrieval in citrate buffer. The endogenous peroxidase activity on the sections was blocked using 3% H_2O_2 solution followed by blocking with 10% donkey serum for 30 min at room temperature followed by incubation with primary antibodies targeting Ki67 (1:2000; Proteintech, 27309-1-AP) and OLFM4 (1:200; CST, #39141) at 4 °C overnight. The secondary antibody was applied the next day, diaminobenzidine (DAB; Solarbio, DA1015) and hematoxylin were used for nuclei staining.

For immunofluorescence assays, sections were incubated with 10% donkey serum for 30 min after dewaxing and antigen retrieval. Then, sections were incubated with primary antibodies targeting GFP (1:200; Abcam, ab6673), LGR5 (1:200; Abclonal, A10545), cleaved-CASP3 (1:400; CST, #9664), DCLK1 (1:200; Proteintech, 21699-1-AP), Lysozyme (1:200; Abclonal, A0641), MUC2 (1:200; GeneTex, GTX100664), and HYOU1(1:100; Santa Cruz sc-398,224) at 4 °C overnight. Sections

were stained with secondary antibodies (1:200; Servicebio) for 1 h at room temperature. For ulex europaeus agglutinin-1 (UEA-1, 1:200; Vector Laboratories, DL-1067-1) staining, sections were incubated with UEA-1 for 1 h at 37 °C. The nuclei were stained with 4,6-diamidino-2-phenylindole (DAPI; Solarbio, C0065) at room temperature for 5 min. Images were captured with an inversion fluorescence microscope (Axio Observer 7, Carl Zeiss).

2.4. Organoids isolation, culture and treatment

Crypts were isolated as previously described with minor modifications [34]. Briefly, after removal of external membrane and fat, intestines segments from ileum were opened longitudinally and flushed with cold PBS thoroughly in a 10 cm dish. The intestine was cut into 2 mm pieces into a 50 mL conical tube and washed with cold PBS for approximately 15 times until the supernatant is clear. The tissue pieces were resuspended and incubated with the Gentle Cell Dissociation Reagent (STEMCELL Technologies, #07174) at room temperature for 15 min on a rocking platform at 20 rpm. To enrich crypts, tissue suspension was filtered through 70-μm nylon mesh, washed with cold PBS containing 0.1% BSA and centrifuged. The isolated crypts were counted and plated 50 μL Matrigel droplets (a mixture of 25 μL undiluted Matrigel® Matrix (Corning, #354277) and 25 μL Mouse IntestiCult™ Organoid Growth Medium (STEMCELL Technologies, #06005)) of the 500-crypt suspension into the center of each well of the pre-warmed 24-well plate. After placing the plate at 37 °C for 20 min, 500 μL IntestiCult™ Organoid Growth Medium was added to each well and the plate was incubated at 37 °C and 5% CO_2. The culture medium was replaced every three days. The surface area of organoids was captured by taking randomized photos using an inverted microscope (Axio Observer 7, Carl Zeiss). Organoids were exposed every 3 days with lipopolysaccharide (LPS; Sigma-Aldrich, L4391), fucose (FUC, 5 mg/mL; Sigma-Aldrich, #354277), and NQDI-1 (5 μM; Selleck, S8289).

2.5. Proliferation assay

Cell proliferation assay was conducted by EdU staining (BeyoClick™ EdU Cell Proliferation Kit with Alexa Fluor 594, Beyotime) following the manufacture's instruction. The pre-warmed EdU working solution was added to the culture medium for 2 h and organoids were then fixed with 4% PFA for 15 min. After washing with PBS, organoids were added with 500 μL Click Reaction Buffer for each well in the dark for 30 min. The fluorescence images were captured with a fluorescence microscope (Axio Observer 7, Zeiss, Germany).

2.6. ROS staining

The ROS level of intestinal organoids was detected by Reactive Oxygen Species Assay Kit (Beyotime, S0033S) according to the manufacture's instruction. Briefly, the DCFH-DA probe was diluted with serum-free medium at 1:1000 and added to the organoids for 30 min at 37 °C. The fluorescence images were captured with a fluorescence microscope (Axio Observer 7, Zeiss, Germany).

2.7. Calcein AM/PI staining

Cell viability of intestinal organoids after treatment was detected by Calcein AM/PI Cell Live/Dead Assay Kit (Beyotime, C2015M). The working solution was prepared following the manufacture's instruction. Organoids seeded in 96-well plates were incubated with 100 μL working solution each well for 30 min at 37 °C. Organoids were then rinsed with PBS and the fluorescence images were captured with a fluorescence microscope (Axio Observer 7, Zeiss, Germany).

2.8. JC-1 probe staining

The mitochondrial membrane potential (MMP) change of intestinal organoids after treatment was detected with JC-1 fluorescent probe (Keygen, KGA603). The working solution was prepared following the manufacture's instruction at 37 °C. Organoids were gently rinsed by PBS once and then incubated with 500 μL working solution for 20 min at 37 °C. After rinsed twice with a pre-cooled buffer solution, the fluorescence images were captured with a fluorescence microscope (Axio Observer 7, Zeiss, Germany). The mitochondria with higher potential were labeled with red fluorescence. The mitochondria with lower potential, which indicate an early stage of apoptosis, were labeled with green fluorescence. The MMP is expressed as the ratio of red fluorescence intensity to green fluorescence intensity.

2.9. Organoids immunofluorescence staining

Organoids were extracted from Matrigel with Cell Recovery Solution (Corning, S0033S) and fixed with 4% PFA. Organoid suspensions were centrifuged at 290 g for 5 min to remove the PFA, washed with PBS and pelleted. Then, the organoids were spread on glass slides. Attached organoids were permeabilized with 0.3% Triton X-100 in PBS for 15 min and blocked with 5% bovine serum albumin for 1 h. Samples were then incubated overnight with the primary antibodies targeting GRP78 (1:200; Proteintech, 11587-1-AP), GFP (1:200; Abcam, ab6673), and γH2AX (1:200; CST, #9718). Slides were then stained with the corresponding secondary antibodies (1:200; Servicebio) for 1 h at room temperature and counterstained with DAPI for 10 min. The representative images were captured with a fluorescence microscope (Axio Observer 7, Zeiss, Germany).

2.10. RNA extraction and PCR analysis

RNA was extracted from intestine tissue or intestinal organoids using TRIzol reagent (15596018, Invitrogen) according to the manufacturer's protocol. The reverse transcription (cDNA) was synthesized from 1 μg of total RNA with PrimeScript RT Master Mix Kit (Takara, RR036A). The real-time polymerase chain reactions (RT-PCRs) were conducted with the SYBR Premix Ex Taq (TaKaRa, RR420A) and Roche LightCycler R480 transcript analyzer (Roche, Switzerland). The relative fold change of mRNA expression was performed using the $2^{-\Delta\Delta CT}$ method. The expression level was normalized to that of the house-keeping gene, β-actin. Primers used for qPCR were shown in Supplementary Table S1.

2.11. Western blot and UEA-1 chromatography

Proteins were extracted from intestinal organoids and intestine tissues with RIPA lysis buffer (Servicebio, G2002) supplemented with phenylmethyl sulfonyl fluoride (PMSF; Servicebio, G2008) protease inhibitor and phosphatase inhibitor (Servicebio, G2007). Protein concentration was measured using the BCA kit (Servicebio, G2026). Total proteins were subjected to sodium dodecyl sulfate polyacrylamide gel electrophoresis (SDS-PAGE) and then transferred to PVDF membranes (Millipore, IPVH00010). Then membranes were later blocked with 5% skimmed milk. After blocking, the membranes were incubated overnight at 4 °C with the corresponding primary antibodies of ACTB (1:2000; Proteintech, 66009-1-Ig), LGR5 (1:1000; Abclonal, A10545), OLFM4 (1:1000; CST, #39141), ZO-1 (1:2000; Proteintech, 21773-1-AP), OCCLUDIN (1:1500; Proteintech, 27260-1-AP), FUT2 (1:1000; Biorbyt, orb 156968), CASP3 (1:1000; Proteintech, 19677-1-AP), BCL2 (1:1000; Proteintech, 26593-1-AP), BAX (1:1000; CST, #2772), CYTC (1:1000; CST, #4280), HYOU1 (1:200; Santa Cruz, sc-398,224), GRP78 (1:1500; Proteintech, 11587-1-AP), IRE1 (1:1000; Proteintech, 27528-1-AP), p-IRE1 (1:1000; Abcam, ab124945), TRAF2 (1:1000; Proteintech, 26846-1-AP), ASK1 (1:1000; Proteintech, 28201-1-AP), p-ASK1 (1:500; Affinity, #AF3477), JNK (1:3000; Proteintech, 24164-1-AP), *p*-JNK

(1:1500; Proteintech, 80024-1-RR), XBP1 (1:1000; Abcam, ab220783), CHOP (1:1000; Abcam, ab11419), ATF6 (1:1000; Proteintech, 24169-1-AP), and POMT2 (1:1000; Invitrogen, PA5-51987). HRP-conjugated secondary antibodies (1:5000; Proteintech, SA00001-1, SA00001-2) were then applied. Protein bands were visualized by the FluorChem Imaging System (ProteinSimple, San Jose, California, USA) using the enhanced chemiluminescence detection kit (Affinity, KF003) to the membranes. The integrated density of each blot was measured using ImageJ software. For UEA-1 chromatography, cells were lysed with cold IP cell lysis buffer (Beyotime, P0013) as previously described with minor modifications [35]. A total of 500 μg of lysate was mixed with 50 μL of agarose-bound UEA-1 (Vector Laboratories, AL-1063-2), diluted the lysate solution to 500 μL with PBS and incubated with rotation at 4 °C overnight. Beads were washed and subsequently extracted with 5× SDS-PAGE loading buffer for further immunoblotting assay.

2.12. Fluorescence-activated cell sorting

Fluorescence activated cell sorting (FACS) was performed using a MoFlo XDP cell sorter from Beckman Coulter. The isolated crypts from WT and *Fut2*$^{\Delta ISC}$ mice were incubated with *anti*-GFP, re-suspended in ice-cold PBS, filtered with 70 mm filters and sorted using the FACS sorter. The GFP^{+} cells were sorted out for subsequent proteomics experiments.

2.13. TMT-labeled quantitative proteomics and N-linked glycosylation modification quantitative proteomics

Cell samples were sonicated three times on ice by a high intensity ultrasonic processor (Scientz) in lysis buffer (8 M urea, 1% protease inhibitor cocktail) and centifuged at 12,000 g at 4 °C for 10 min, the protein concentration was examined with BCA kit. The lysate was reduced with 5 mM dithiothreitol for 30 min at 56 °C and alkylated with 11 mM iodoacetamide for 15 min at room temperature in the dark. The trypsin was added to the protein solution overnight and then the peptides were desalted by C18 SPE column. Each channel of peptide was labeled with their respective TMT reagent (based on manufacturer's protocol, ThermoFisher Scientific), and incubated for 2 h at room temperature. The sample was fractionated into fractions by high pH reverse-phase HPLC using Agilent 300 Extend C18 column (5 μm particles, 4.6 mm ID, 250 mm length).

Then, for quantitative proteomics analysis, the tryptic peptides were dissolved in solvent A (0.1% formic acid, 2% acetonitrile/in water) and separated using an EASY-nLC 1200 ultra performance liquid system. The separated peptides were analyzed in Q ExactiveTM HF-X (ThermoFisher Scientific) with a nano-electrospray ion source.

For *N*-linked glycosylation modification quantitative proteomics, after labeled with TMT regent and fractionated by HPLC, the peptides were redissolved in 200 μL washing buffer (80% IN, 5% TFA) and then loaded onto the column. Glycopeptides were eluted with 0.1% TFA, 50 mM ammonium bicarbonate and 50%IN for two times. The eluted glycopeptides were dried and redissolved with 50 μL of 50 mM ammonium bicarbonate solution dissolved in H_2O^{18}. After adding 2 μL of PNGase F glycosidase, the digestion was performed at 37 °C overnight and desalted for further MS analysis. The LC-MS/MS analysis was conducted by Jingjie PTM BioLab (Hangzhou, China). The resulting MS/MS data were processed using MaxQuant search engine (v.1.6.15.0). Tandem mass spectra were searched against the human SwissProt database (20,422 entries) concatenated with reverse decoy database. The expression changes of glycosylation modified proteins were calculated based on the results of TMT-labeled quantitative proteomics.

2.14. Bioinformatics analysis

To further analyze the results of *N*-glycoproteomics, the Gene Ontology (GO) analysis was used to annotate protein's GO function and classify the differentially expressed proteins (DEPs) based on three categories, biological process, cellular component, and molecular function. For subcellular localization analysis, wolfpsort, a subcellular localization predication soft, was used to predict subcellular localization. For motif analysis, Momo application was used to analyze motif characteristics of modified sites based on the motif-x algorithm. The bioinformatics was plotted by https://www.bioinformatics.com.cn for data visualization.

2.15. Site-directed mutagenesis

As analyzed by *N*-glycoproteomics, HYOU1 has a predicted *N*-glycosylation consensus site located at the site of asparagine 862 (Asn862 or N862). The site-directed mutagenesis (Tsingke Biotechnology) was used to generate a new expression HYOU1 construct with the cloning vector pCDNA3.1 which encoded a replacement of asparagine by glutamine at position 862, referred to as HYOU1 N862Q with the vector pCDNA3.1. The transfection protocol was previously described [36] with some modifications. The organoids were rinsed with Gentle Cell Dissociation Reagent (STEMCELL Technologies, #07174), resuspended in growth medium and plated in 48-well plates. The prepared DNA-Lipofectamine 3000 reagent (Invitrogen, L3000001) complexes in Opti-MEM medium were incubated for 5 min and added to the cells. The plates were centifuged and incubated for 4 h at 37 °C before plated in Matrigel.

2.16. Statistical analysis

All data were presented as the mean ± square deviation. At least 3 independent experiments were conducted, and the data were analyzed using GraphPad Prism (GraphPad Software Inc, USA). Student's t-tests were performed to analyze the statistical significance between two groups. Statistical significance among multiple groups was determined by multiple comparisons with ANOVA followed by Tukey post hoc tests and multiple comparisons. *, $P < 0.05$ was considered statistically significant.

3. Results

3.1. Fucose alleviates intestinal inflammatory injury and ISC damage

Improvement of DSS-induced intestinal injury by fucose treatment was noted in this project. Based on the daily document, we found the mice in the DSS + FUC group showed significantly lower changes in body weight loss and disease activity index (DAI) scores than the DSS group (Fig. 1A and B). Histological analysis showed that fucose ameliorated DSS-induced destruction of the intestinal epithelial structure, including glandular defects, inflammatory cell infiltration, mucosal ulceration, and crypt destruction (Fig. S1A). The barrier function, reflected by tight junction proteins including OCCLUDIN and ZO-1, was destroyed by DSS while restored by fucose treatment (Figs. S1C and D). DSS triggered an inflammatory response while fucose downregulated the mRNA levels of pro-inflammatory factors such as *Tnfα* and *Il1β* (Fig. S1B). Moreover, the apoptosis change in the intestinal epithelium was detected and less cleaved-CASPASE3 (cleaved-CASP3) positive cells in the DSS + FUC group was observed than that of the DSS group (3.39 ± 1.10% vs. 11.00 ± 2.09%; $P < 0.001$), especially in the basal crypt area (Fig. 1C and D).

Intestinal stem cells (ISCs) at the base of crypts exert a central role in epithelial repair and regeneration, thus we speculated that DSS-induced destruction of intestinal epithelial might resulted from the loss or dysfunction of ISCs. As widely reported, OLFM4 and LGR5 are among the biomarkers of ISCs. Here, the positive rate of OLFM4 cells per crypt was remarkably decreased in the DSS group compared to the DSS + FUC group (7.44 ± 2.23% vs. 17.10 ± 2.02%; Fig. 1E). Meanwhile, the number of LGR5-positive cells (Fig. 1G) and the protein level of LGR5

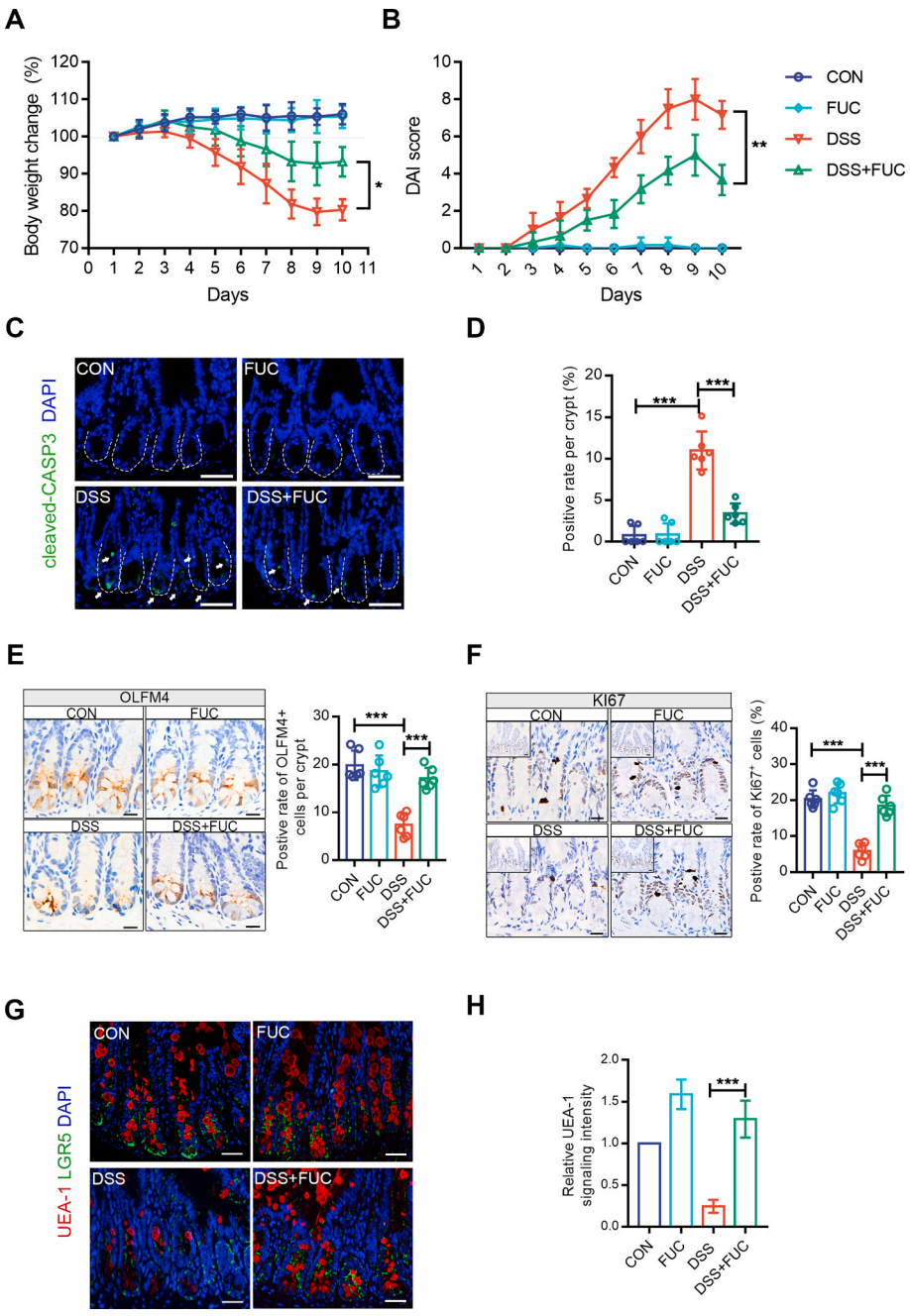

Fig. 1. The protective effects of fucose on intestinal stem cells against DSS-induced injury. (A) The body weight change was documented every day in the process of DSS and fucose (FUC) administration. (B) Disease activity index (DAI) evaluations of mice. (C) Immunofluorescence staining of cleaved-CASP3 in intestine sections. The positive staining cells were indicated by white arrowheads. The nucleus was labeled with DAPI. Scale bar: 50 μm. (D) The positive rate of cleaved-CASP3 was shown in the statistical chart. (E) Immunohistochemistry staining of OLFM4 in intestine sections for each group. Scale bar: 20 μm. The positive rate of OLFM4 per crypt was analyzed in the right statistical chart. (F) Immunohistochemistry staining of Ki67 in intestine sections. Scale bar: 20 μm. The positive rate of Ki67 was analyzed in the right statistical chart. (G) Typical images of mice intestine tissues stained with UEA-1 (red). The ISCs were labeled with LGR5 (green). Scale bar: 20 μm. (H) The relative UEA-1 signaling intensity (normalized to the CON group) was analyzed in the statistical chart. The results were representative of at least three times independent experiments. Results were shown as mean ± SD. $^{*}P < 0.05$, $^{*}P < 0.01$, $^{***}P < 0.001$. (For interpretation of the references to colour in this figure legend, the reader is referred to the Web version of this article.)

(Fig. S1D) were restored by fucose under DSS conditions. Besides, higher levels of Ki67 at the bottom of the crypts in the DSS + FUC group compared with the DSS group (5.86 ± 1.93% in the DSS group vs. 18.48 ± 2.57% in the DSS + FUC group, $P < 0.001$) revealed that fucose sustained the proliferation capacity against intestinal injury (Fig. 1F). UEA-1 staining exhibited the higher level of α-1,2-fucosylation in the intestine epithelium of mice exposed to fucose, while DSS alone significantly suppressed the level of α-1,2-fucosylation (Fig. 1G and H). In agreement with the fucosylation alternation, the expression of FUT2 was also upregulated by fucose treatment in intestinal tissue (Figs. S1C and D).

3.2. Fucose mitigates LPS-induced intestinal organoids injury

To better understand the precise role of ISCs in controling intestinal homeostasis and epithelial repair, we evaluated the functions and survival of ISCs by *ex vivo* assays using intestinal organoids [37]. The intestinal injury model on organoids was established by LPS to investigate the biological characteristics of ISCs in response to inflammatory stimuli. Primary intestinal organoids were treated with different concentrations of LPS (0, 0.1, 1, 5, and 10 μg/mL) continuously for 6 days. LPS of 5 μg/mL significantly reduced the number of organoid buds (Figs. S2A and B). Then LPS of 5 μg/mL was used for further experiments.

To investigate the protective effects of fucose against LPS-induced injury, alternations of the inflammatory response including oxidative stress, mitochondrial dysfunction, and apoptosis were assessed. Reactive oxygen species (ROS) levels were detected by the DCFH-DA probe and fucose remarkably attenuated the ROS fluorescence signal which was stimulated by LPS (Fig. 2A and B). Calcein AM/PI double staining suggested that LPS increased the number of dead cells (PI-positive) while fucose reduced the PI positive rate, indicating that fucose could

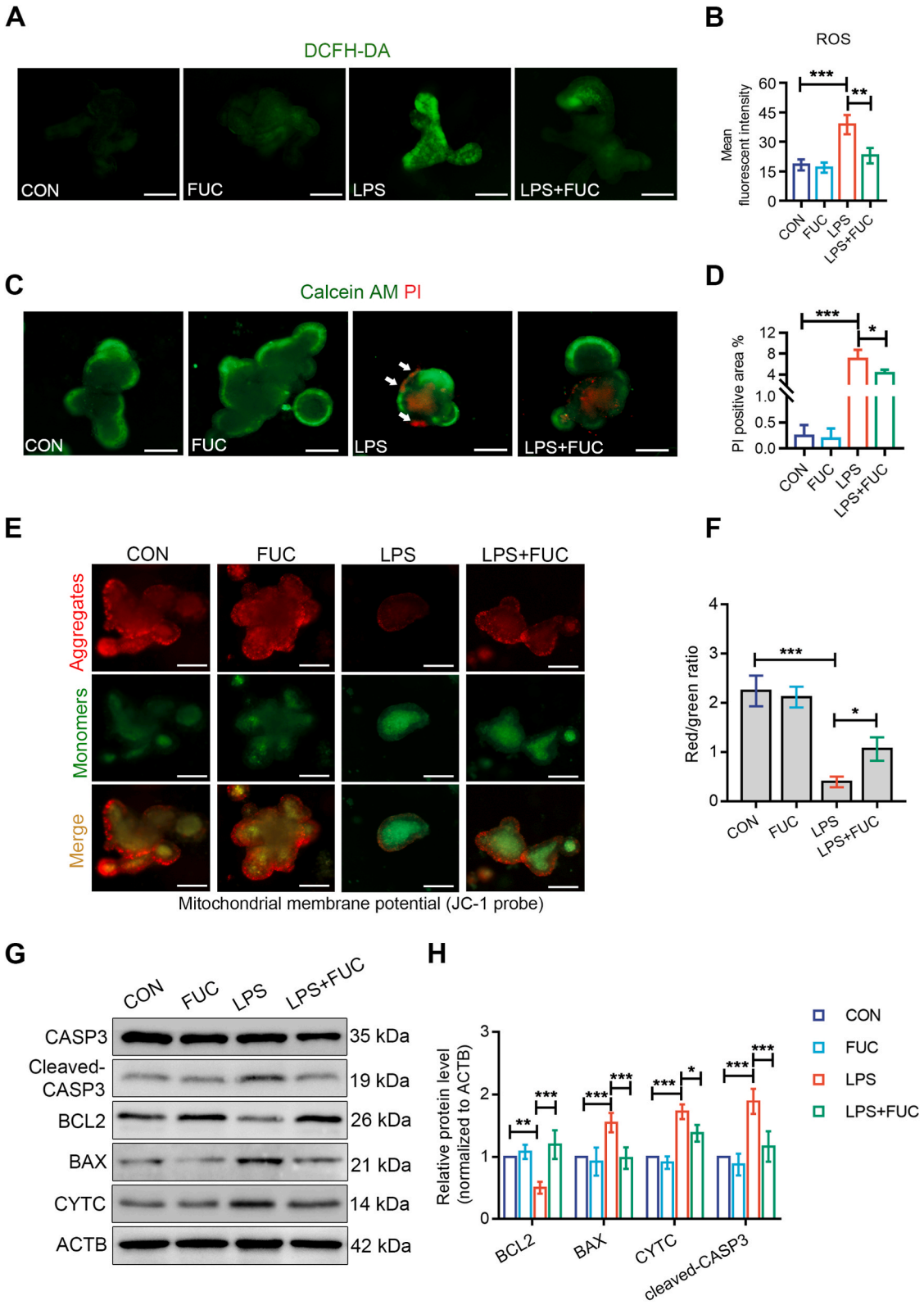

Fig. 2. The effects of fucose against LPS-induced oxidative stress and cell death in the intestinal organoids. (A) The ROS staining of intestinal organoids treated with LPS and FUC was detected by the DCFH-DA probe. Scale bar: 50 μm. (B) The mean fluorescent intensity of ROS was analyzed in the statistical chart. (C) Calcein AM/PI double staining showed the changes in cell death for each group. Calcein AM staining showed green fluorescence in living cells. Propidium Iodide (PI) stained dead cells, presenting red fluorescence. Scale bar: 50 μm. (D) The ratio of PI positive area to Calcein AM positive area was analyzed. (E) The JC-1 probe staining of intestinal organoids treated with LPS and FUC. The changes of JC-1 from red fluorescence (JC-aggregates) to green fluorescence (JC-monomers) indicate the decrease of mitochondrial membrane potential (MMP). Scale bar: 50 μm. (F) Statistical analysis of MMP changes, indicated by the red/green ratio in intestinal organoids. (G) Western blot analysis of apoptosis-related proteins, including cleaved-CASP3, BAX, BCL2, and CYTC in intestinal organoids. (H) Densitometric analysis of apoptosis-related proteins in organoids treated with LPS and FUC. At least 3 independent experiments were conducted. Results were shown as mean ± SD. $^{*}P < 0.05$, $^{*}P < 0.01$, $^{***}P < 0.001$. (For interpretation of the references to colour in this figure legend, the reader is referred to the Web version of this article.)

ameliorate LPS-induced cell death (Fig. 2C and D). To further explore how LPS triggered cell death, mitochondrial membrane potential (MMP) was assessed by the JC-1 probe to evaluate the mitochondrial function and the changes of early apoptosis (Fig. 2E). Fucose restored the decrease of MMP caused by LPS stimulation, indicated by the ratio of red (JC-1 aggregates) to green fluorescence (JC-1 monomers) (Fig. 2F). The generation of ROS and reduction of MMP concurrently attributed to early programmed cell death and triggered the activation of mitochondrial apoptosis pathway, as shown by the LPS-induced up-regulation of BAX, CYTC, cleaved-CASP3, and down-regulation of BCL2 in blotting experiments (Fig. 2G and H). These data revealed the protective effects of fucose against LPS-induced oxidative stress and cell apoptosis in the

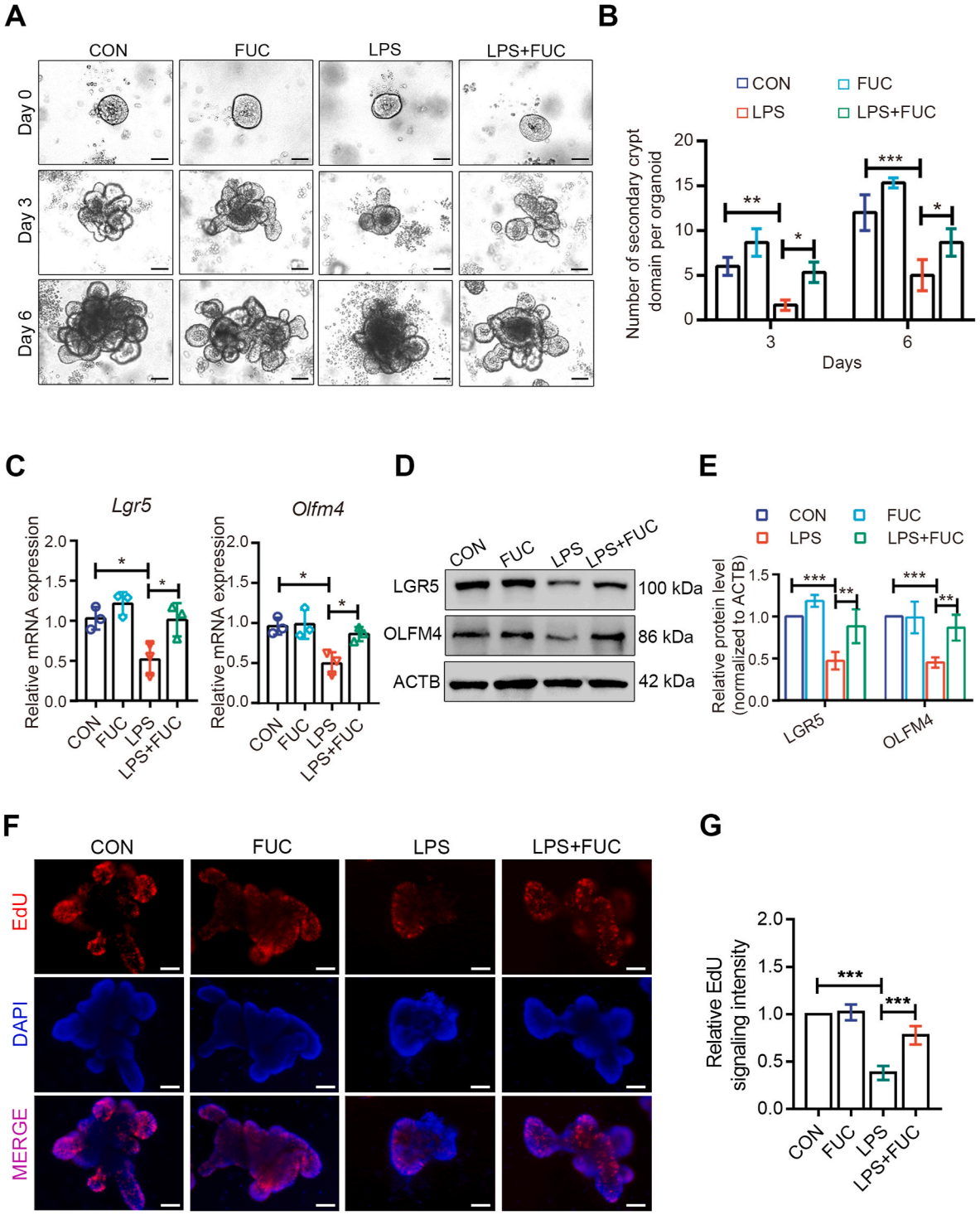

Fig. 3. Stemness and proliferation capacity restoration in organoids treated with fucose. (A) Representative images of intestinal organoids exposed to LPS and FUC on day 0, 3, and 6. Scale bar: 50 μm. (B) Quantification and statistical analysis of the organoid buddings on day 3 and day 6. (C) The relative mRNA expression of stem cell markers *Lgr5* and *Olfm4* in intestinal organoids. (D) Western blot analysis of LGR5 and OLFM4 in intestinal organoids. (E) Densitometric analysis of LGR5 and OLFM4 was shown in the statistical chart. (F) EdU staining of intestinal organoids treated with LPS and FUC. (G) The relative EdU signaling intensity (normalized to the CON group) was analyzed in the statistical chart. At least 3 independent experiments were conducted. Results were shown as mean ± SD. $^{*}P < 0.05$, $^{*}P < 0.01$, $^{***}P < 0.001$.

intestinal organoids.

3.3. Fucose maintains stemness and proliferation capacity of intestinal epithelium

In order to explore how fucose tuned the function of ISCs, the potential of organoid budding which reflected the self-renewal ability of ISCs was examined. Intestinal organoids exhibited a constant state of impaired growth in the presence of LPS whereas fucose supplementation significantly restored the number of organoid buds during LPS stimulation (Fig. 3A and B). The mRNA levels of stemness related genes including *Lgr5* and *Olfm4* were restored by fucose upon LPS-induced stemness loss (Fig. 3C). This was further confirmed by the same protein expression patterns of LGR5 and OLFM4 (Fig. 3D and E). Besides, LPS-treated organoids exhibited diminished EdU signaling intensity, an indicator of proliferation capacity, when compared to the CON group. The defective proliferation capacity of ISCs was regained by fucose under LPS conditions (Fig. 3F and G). Collectively, these results concurrently revealed that fucose maintained the stemness and proliferation capacity of ISCs against LPS-induced injury.

3.4. FUT2 is required for ISCs proliferation and survival upon inflammatory injury

Consistent with *in vivo* results, FUT2 was upregulated both at mRNA and protein levels when exposed to fucose (Fig. 4A and B). The intestinal organoids derived from *Lgr5-EGFP-IRES-Cre^{ERT2}* mice were used for UEA-1 staining (Fig. 4C). GFP-positive ISCs exhibited a higher level of co-localized red fluorescence when exposed to fucose, while LPS alone debilitated UEA-1 signaling throughout the integral organoids as well as in the GFP-positive area (Fig. 4D). Thus, to further explore the effect of FUT2-mediated fucosylation on ISCs, we crossed *Fut2$^{fl/fl}$* mice with *Lgr5-EGFP-IRES-Cre^{ERT2}* mice to generate the *Lgr5-eGFP-IRES-Cre^{ERT2}/Fut2$^{fl/fl}$* mice (*Fut2$^{\Delta ISC}$*) of inducible *Fut2* specifically knockout in ISCs.

Organoids from *Fut2$^{\Delta ISC}$* and WT (*Lgr5-EGFP-IRES-Cre^{ERT2}*) mice were isolated and concurrently treated with LPS and fucose. The number of organoid buds in the LPS + FUC treated *Fut2$^{\Delta ISC}$* group was significantly lower than that of the LPS + FUC treated WT group (3.40 ± 1.02 vs. 9.20 ± 1.72, $P < 0.001$) (Fig. 5A and B). Besides, the mRNA levels of stem cell markers *Lgr5* and *Olfm4* were restored by fucose in the WT organoids but not in the *Fut2$^{\Delta ISC}$* organoids (Fig. 5C), indicating that FUT2 depletion in ISCs caused severe growth and stemness defects of intestinal organoids. EdU staining revealed that FUT2 depletion exacerbated the impaired proliferation capacity induced by LPS and blocked the protective effects of fucose, as shown in the figure that the EdU signaling intensity was notably higher in the WT group treated with LPS + FUC than in the *Fut2$^{\Delta ISC}$* group with the same treatment ($P < 0.001$; Fig. 5D and E). In addition, FUT2 depletion hindered the potential of ISCs to differentiate into Paneth cells, goblet cells, and tuft cells (Fig. S3). Therefore, FUT2 was identified as the critical effector of fucose for modulating ISC self-renewal and stemness. Meanwhile, a lower level of JC-1 aggregates labeled red fluorescence was detected in the *Fut2$^{\Delta ISC}$* groups under inflammatory conditions, suggesting the aggravation of mitochondrial dysfunction and MMP loss (Fig. 5F). The red/green signaling ratio in the *Fut2$^{\Delta ISC}$* organoids showed no remarkable difference between the LPS group and the LPS + FUC group (0.26 ± 0.07 vs.

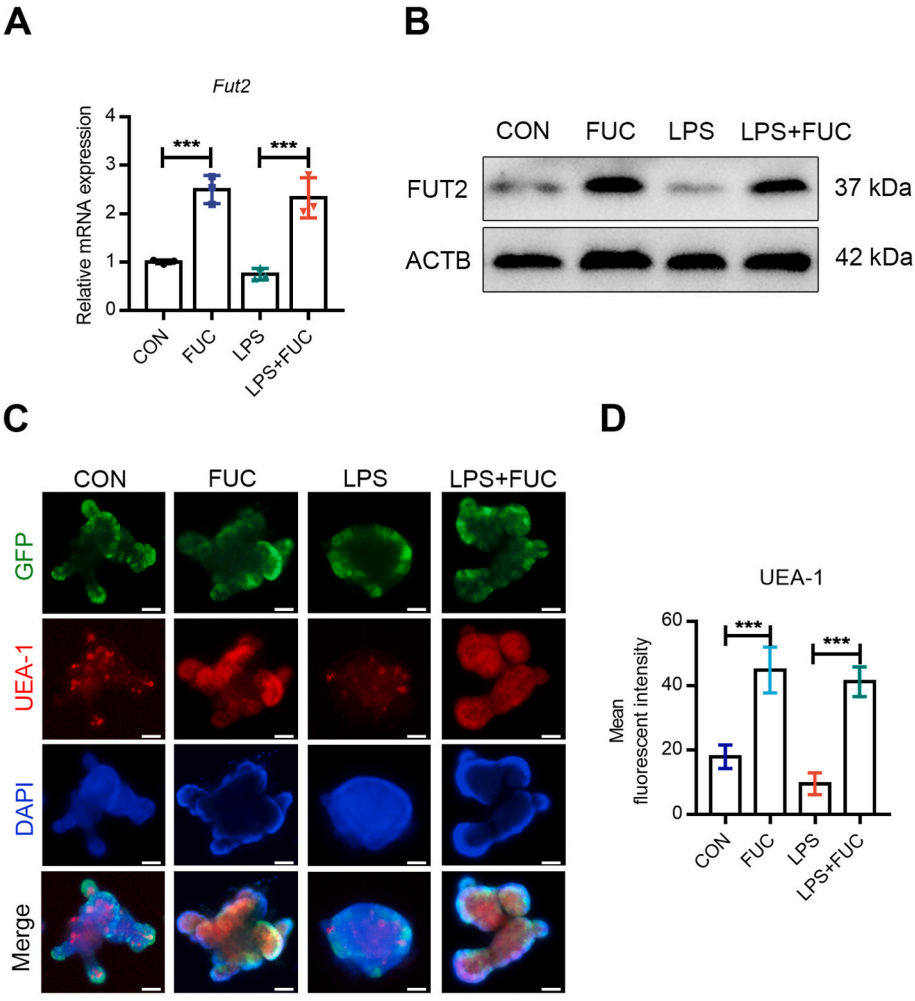

Fig. 4. The level of FUT2 and α-1,2-fucosylation in intestinal organoids. (A) The relative mRNA expression of *Fut2* in intestinal organoids for each group. (B) Western blot analysis of FUT2 in intestinal organoids. (C) Typical images of intestinal organoids stained with UEA-1 (red); the intestinal stem cells (ISCs) were labeled with GFP (green). Scale bar: 50 μm. (D) The mean fluorescent intensity of UEA-1 was analyzed in the statistical chart. At least 3 independent experiments were conducted. Results were shown as mean ± SD. *$P < 0.05$, *$P < 0.01$, ***$P < 0.001$. (For interpretation of the references to colour in this figure legend, the reader is referred to the Web version of this article.)

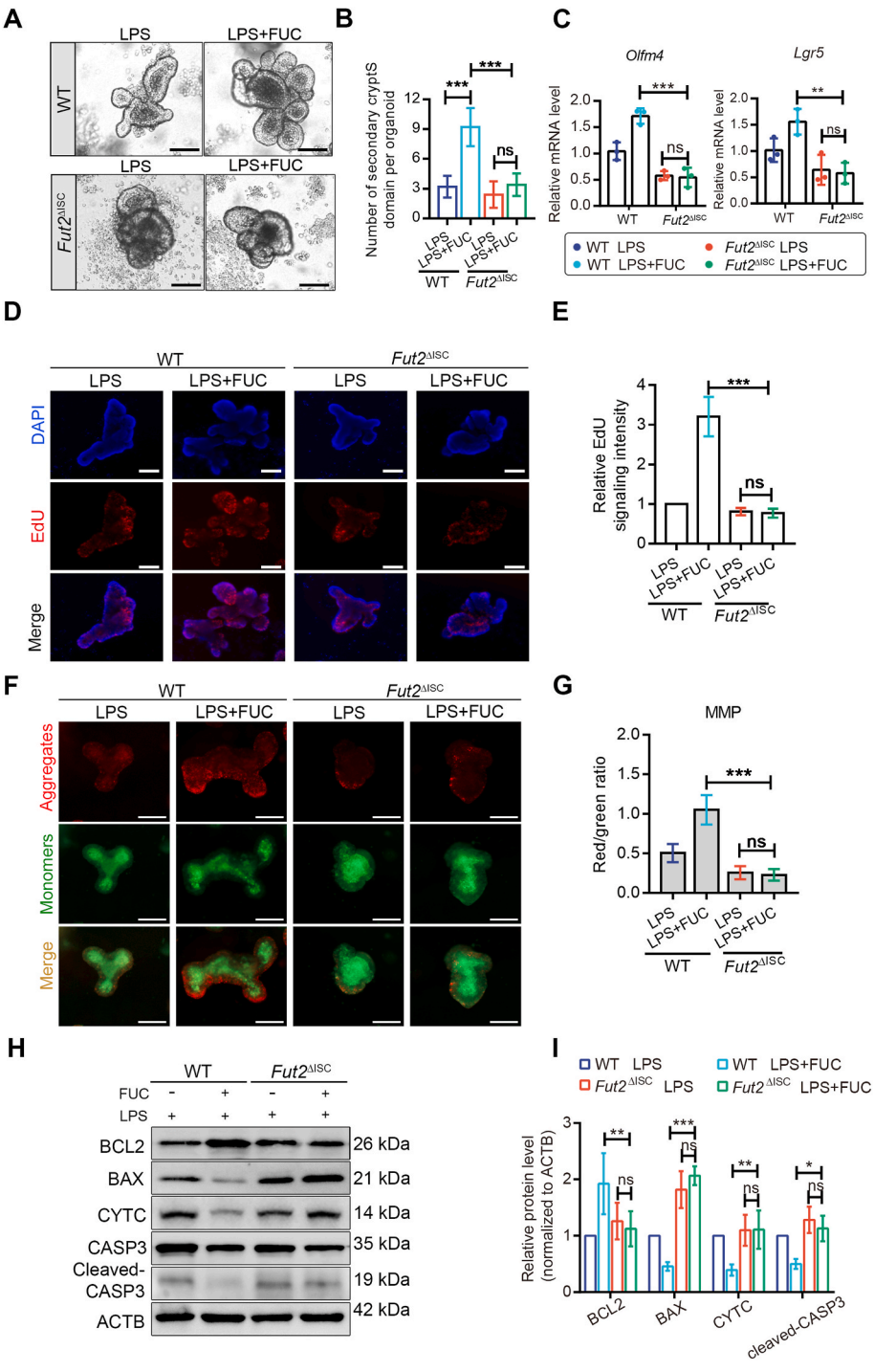

Fig. 5. FUT2 activation in control of proliferation and survival of intestinal stem cells. (A) Representative images of intestinal organoids from WT and *Fut2*$^{\Delta ISC}$ mice exposed to LPS and FUC. Scale bar: 50 μm. (B) Quantification and statistical analysis of the organoid buddings was shown in the right statistical chart. (C) The relative mRNA expression of *Lgr5* and *Olfm4* in intestinal organoids treated with LPS and FUC. (D) EdU staining of intestinal organoids from WT and *Fut2*$^{\Delta ISC}$ mice treated with LPS and FUC. Scale bar: 100 μm. (E) The relative EdU signaling intensity (normalized to the LPS-treated WT group) was analyzed in the statistical chart. (F) The JC-1 probe staining of intestinal organoids treated with LPS and FUC. Scale bar: 100 μm. (G) Quantitative analysis of the red/green ratio was shown in the statistical chart. (H) Western blot analysis of apoptosis-related proteins, including cleaved-CASP3, BAX, BCL2, and CYTC in WT and *Fut2*$^{\Delta ISC}$ intestinal organoids. (I) Densitometric analysis of apoptosis-related proteins in WT and *Fut2*$^{\Delta ISC}$ organoids was shown in the statistical chart. The relative protein level was normalized to the LPS-treated WT group. At least 3 independent experiments were conducted. Results were shown as mean ± SD. ns, non-significant; *$P < 0.05$, *$P < 0.01$, ***$P < 0.001$. (For interpretation of the references to colour in this figure legend, the reader is referred to the Web version of this article.)

0.23 ± 0.06, $P > 0.05$) (Fig. 5G). This result was further verified by the Western blot experiments that FUT2 depletion eliminated the advantageous role of fucose on restraint of mitochondrial apoptosis pathway, including the downregulation of BCL2 and the upregulation of BAX, CYTC, and cleaved-CASP3 (Fig. 5H and I). Consequently, these data elucidated the crucial requirements of FUT2 in ISCs to safeguard proper growth and proliferation against harmful stimuli-induced cell damage.

3.5. *N*-glycoproteomics reveals cellular response and target glycoproteins regulated by FUT2 in ISCs

To further decipher the regulatory mechanisms of FUT2 in the maintenance of ISC homeostasis, we used a quantitative proteomics approach to gain an integrated view of the *N*-linked glycosylation alternations in response to FUT2 depletion in ISCs. ISCs labeled with GFP were isolated using the fluorescence-activated cell sorting (FACS) method and then applied LC-MS/MS analysis (Fig. 6A). The expression changes of differential glycosylated proteins were normalized to the changes of corresponding proteins in proteomics (Figs. S4A and B). A total of 201 *N*-glycosylation sites in 162 differential glycoproteins were identified (Fig. 6B). *N*-glycosylation motif analysis showed that the most significantly enriched motif was the classical *N*-glycosylation sequence: *N*-X-S (Fig. 6C). Gene Ontology (GO) analysis revealed that FUT2-dependent *N*-glycoproteins changes were involved in diverse

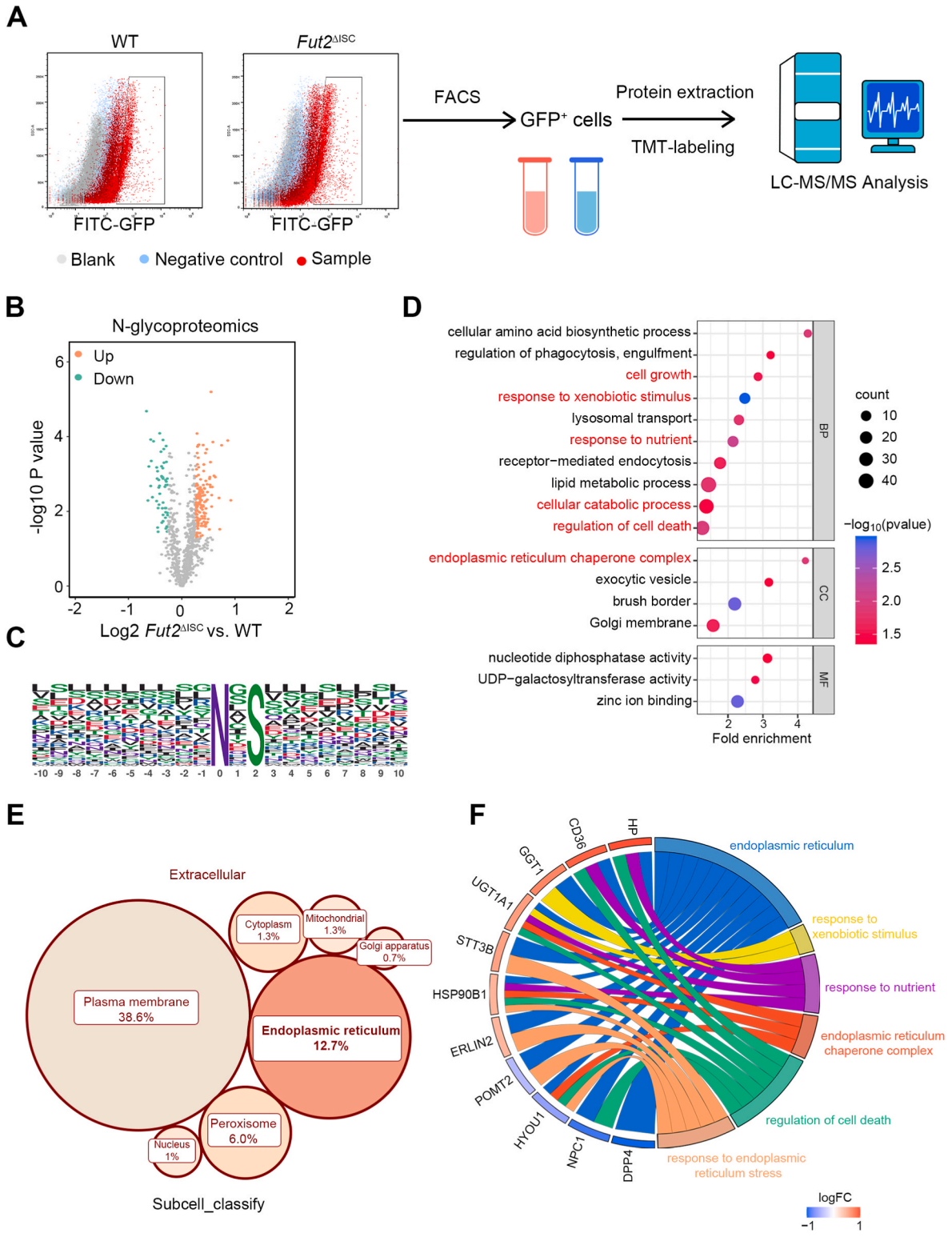

Fig. 6. Identification of FUT2-mediated cellular response and the target glycoproteins by *N*-glycoproteomics. (A) Schematic illustration of the experimental procedures to identify differential *N*-glycoproteins between WT and *Fut2*$^{\Delta ISC}$ ISCs. The GFP-labeled ISCs were derived from WT and *Fut2*$^{\Delta ISC}$ mice and sorted by fluorescence-activated cell sorting using *anti*-GFP antibody. GFP-positive cells were then examined by LC-MS/MS analysis. (B) Volcano plot depicting the differentially expressed glycoproteins between WT and *Fut2*$^{\Delta ISC}$ ISCs by *N*-glycoproteomics. The ratio cutoff of their expression level (*Fut2*$^{\Delta ISC}$ vs. WT) was set as >1.200 (upregulated) or <0.833 (downregulated). (C) Motif analysis of glycosylation sites identified in *N*-glycoproteomics analysis. (D) GO analysis of differentially expressed glycoproteins, including biological process (BP), cell component (CC), and molecular function (MF). The interested GO terms were marked in red. (E) The classification of subcellular localization of differentially expressed glycoproteins. (F) The GO chordal graph showed the connection between the interested GO enrichment terms with the relevant differentially expressed glycoproteins. (For interpretation of the references to colour in this figure legend, the reader is referred to the Web version of this article.)

biological processes, including regulation of cell death, response to xenobiotic stimuli, cell growth, and response to nutrient, which were strongly associated with the effect that fucose exerted. The endoplasmic reticulum chaperone complex was the notably differentially expressed cellular component (Fig. 6D). Moreover, subcellular classification analysis implied that the endoplasmic reticulum (ER) was the primary organelle where differentially expressed glycoproteins are localized (Fig. 6E). As the main site of *N*-glycoproteins biosynthesis, folding, and posttranslational modification, the ER is often disturbed by multiple cellular perturbations such as inflammatory stimuli, defective glycosylation, and altered redox status that alter ER homeostasis and trigger ER stress [15]. Therefore, it led us to speculate whether FUT2 depletion in ISCs could cause the accumulation of misfolded glycoproteins, trigger ER stress, and then initiate UPR. Thus, based on the above inferences, we analyzed several biological processes closely related to the ER by the GO chordal graph, and the interested differentially expressed glycoproteins were screened out as candidate molecules, which might play a role in counteracting inflammatory injury through FUT2-dependent fucosylation (Fig. 6F).

3.6. Fucose restrains LPS-induced ER stress via IRE1/TRAF2/ASK1/JNK signaling

To elucidate the underlying mechanism of the protective effects of fucose, the stress response of ER was investigated. GRP78 is a vital regulator of the UPR which is induced by ER stress. Under normal conditions, fucose alone did not alter the expression of GRP78. Upon LPS stimulation, fucose remarkably inhibited the upregulation of GRP78 in intestinal organoids (Fig. 7A and B). Thus, ER stress was triggered in response to inflammation accompanied by upregulated GRP78, and UPR was then initiated. To further clarify the specific activated branch of UPR signaling, the mRNA level of representative molecules for each branch was assessed. *Atf6* (belongs to the ATF6 branch), *Atf4*, and *Chop* (belongs to the PERK branch) were not significantly changed. *Traf2*, *Txnip,* and *Xbp1s* of (belongs to the IRE1 branch) were activated by LPS stimulation, while only *Traf2* was restored by fucose treatment, which implied that TRAF2 might be the downstreamer of the IRE1 branch that was indeed regulated by fucose (Fig. 7A). Western blot experiments showed consistent results that the phosphorylated IRE1 was upregulated under LPS stimulation and inhibited by fucose. Activated IRE1 triggered the upregulation of TRAF2, thereby leading to increased levels of phosphorylated ASK1/total ASK1 and phosphorylated JNK/total JNK, while fucose diminished the phosphorylation of these proteins after LPS stimulation (Fig. 7C and D). On the other hand, the protein level of ATF6, ATF4, and CHOP was proved to be not significantly altered (Fig. 7E and F). Taken together, our evidence supported the notion that fucose alleviated LPS-induced injury by modulating the IRE1/TRAF2/ASK1/JNK branch of UPR signaling.

3.7. FUT2 deficiency aggravates IRE1-mediated pro-apoptotic UPR signaling in intestinal organoids

Given our results suggested that fucose attenuated inflammatory injury by inhibiting the pro-apoptotic UPR signaling, we would further investigate how FUT2 regulated UPR in ISCs. The intestinal organoids from WT and *Fut2*$^{\Delta ISC}$ mice were treated with LPS or LPS + FUC, and the expression of UPR proteins was assessed. Notably, FUT2 deficiency in ISCs aggravated the activation of GRP78 in response to LPS stimulation (1.70 ± 0.18 fold of the LPS treated *Fut2*$^{\Delta ISC}$ group to the LPS treated WT group, $P < 0.01$). Besides, GRP78 failed to reach a similarly low level in the LPS + FUC treated *Fut2*$^{\Delta ISC}$ group as in the LPS + FUC treated WT group, indicating that FUT2 deficiency in ISCs blocked the protective effects of fucose on restoring ER homeostasis (Fig. 8A and B). Moreover, the ratio of phosphorylated IRE1, ASK1, and JNK to the corresponding total protein levels were not significant altered between the LPS and the LPS + FUC treated *Fut2*$^{\Delta ISC}$ organoids ($P > 0.05$; Fig. 8A and B). Then, we took a chemical approach to address the function of the IRE1 branch in the intestine organoids using NQDI-1, a selective inhibitor of ASK1. The number of organoid buds was both elevated in WT and *Fut2*$^{\Delta ISC}$ groups with NQDI-1 treatment (Fig. 8C and D). The organoids treated with NQDI-1 exhibited diminished ROS fluorescence intensity both in the WT and *Fut2*$^{\Delta ISC}$ group, which suggested that impeding the activation of ASK1 could alleviate oxidative stress (Fig. 8E). Moreover, the expression levels of *p*-JNK/JNK, cleaved-CASP3, and CYTC were downregulated in the presence of NQDI-1 under both WT and *Fut2*$^{\Delta ISC}$ group (Fig. 8F and G). In summary, we concluded that FUT2 mediated the protective effects of fucose against oxidative stress and apoptosis via the IRE1/TRAF2/ASK1/JNK branch of UPR signaling.

3.8. HYOU1 is the vital fucosylated protein mediated by FUT2

To identify the critical glycoprotein that controlled the UPR signaling of ISCs via FUT2-dependent fucosylation, we focused on the differentially expressed glycoproteins from the dataset of *N*-glycoproteomics and found five of them were involved in the GO terms of UPR and ER stress (Fig. 9A). Among them, the glycosylated HYOU1 and POMT2 were downregulated in the *Fut2*$^{\Delta ISC}$ group, which implied that they were the potential clients fucosylated by FUT2. To validate our glycoproteomics results, we successfully assessed the α-1,2-fucosylation state of POMT2 and HYOU1 by UEA-1 chromatography analysis. The fucosylation level of HYOU1 in ISCs of the WT group was significantly higher than that of the *Fut2*$^{\Delta ISC}$ group, whereas POMT2 showed almost no binding to UEA-1, indicating POMT2 was not fucosylated by FUT2 (Fig. 9B). Of interest, a similar expression pattern of fucosylated HYOU1 was observed in comparison of the WT group to the *Fut2*$^{\Delta ISC}$ group under LPS stimulation. More importantly, fucose enhanced α-1,2-fucosylation of HYOU1 under inflammatory conditions while this effect was completely counteracted by FUT2 depletion (Fig. 9C). In addition, the protein expression level of HYOU1 from whole cell lysates was not significantly altered in the basal conditions while HYOU1 was remarkably upregulated in response to LPS stimulation. To verify the expression of HYOU1 in ISCs *in vivo*, the intestine sections from DSS treated WT mice were stained. We observed that HYOU1 was highly expressed in the DSS group, especially in the GFP-positive cells, while its expression reverted to a relatively low level in the GFP-positive ISCs with fucose treatment (Fig. 9D), which suggested the potential protective role of HYOU1 in response to hostile stimuli.

3.9. Fucosylated HYOU1 enhances ISC resistance to ER stress and injury

Previous research has shown that HYOU1 (also named GRP170 or ORP150), a member of the HSP70 family, acted as a vital nucleotide exchange factor for GRP78 and participated in unfolded or misfolded protein recognition and folding [38]. Therefore, we deduced that fucosylation of HYOU1 may exert essential roles in handling misfolded proteins caused by FUT2 deficiency. Based on the analysis of *N*-glycoproteomics, the significant differentially modification site occurred at asparagine 862 (Asn862 or N862). To validate this prediction, we generated a full-length HYOU1 mutant (HYOU1–N862Q, referred to here as N862Q, and wild-type HYOU1 was referred to here as HYOU1) with the substitution of the N862 to glutamine (Gln, Q) that prevented the attachment of *N*-linked glycans to this specific site. Then UEA-1 affinity chromatography showed that the N862Q mutant blocked the fucosylation of HYOU1 under both LPS and LPS + FUC conditions (Fig. 10A). To validate the role of fucosylated HYOU1 on ISCs under inflammatory conditions, organoids constitutively expressing N862Q and wild-type HYOU1 were cultured with LPS + FUC treatment. De-fucosylated HYOU1 resulted in a decrease in the number of organoids buds (9.83 ± 2.27 in the HYOU1 group compared to 5.83 ± 1.07 in the N862Q group, $P < 0.01$), suggesting that fucosylated HYOU1 at the site of asparagine 862 was closely related to the self-renewal ability of stem cells (Fig. 10B). Immunofluorescence imaging revealed that the

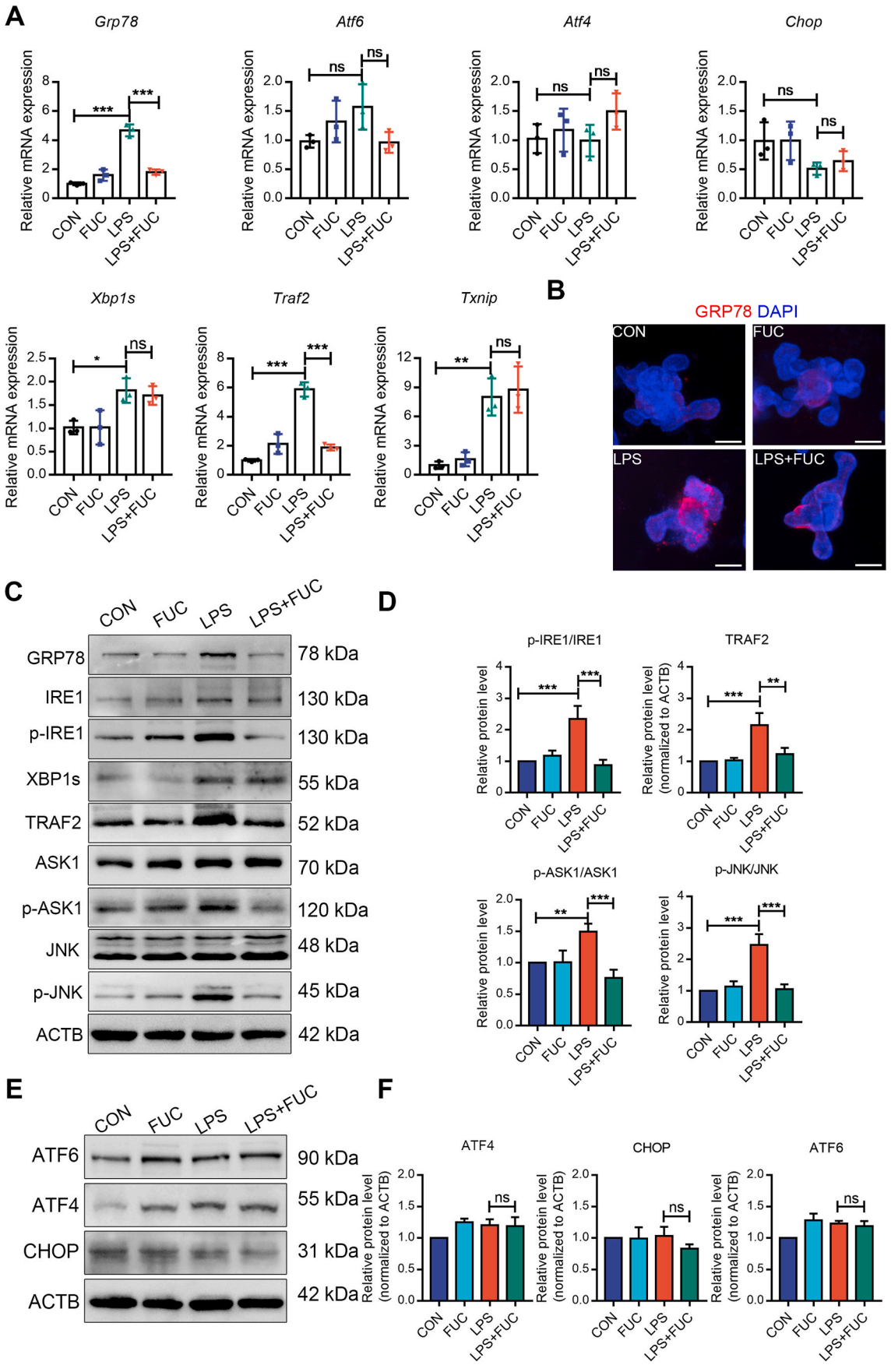

(caption on next page)

Fig. 7. Restraint of LPS-stimulated UPR initiation via IRE1/TRAF2/ASK1/JNK branch by fucose. (A) The relative mRNA expression of UPR-related molecules, including *Grp78*, *Atf6*, *Atf4, Chop*, *Xbp1s*, *Traf2,* and *Txnip* in intestinal organoids treated with LPS and FUC. (B) Immunofluorescence staining of GRP78 in intestinal organoids for each group. Scale bar: 100 μm. (C) Western blot analysis of IRE1 signaling related proteins in the UPR branch. (D) Densitometric analysis of IRE1 signaling-related proteins was shown in the statistical chart. The activation of IRE1, ASK1, and JNK was assessed by calculating the ratio of phosphorylated protein to total protein. The expression of TRAF2 was normalized to ACTB. (E) Western blot analysis of ATF6, ATF4, and CHOP in the UPR branch. (F) Densitometric analysis of ATF6, ATF4, and CHOP in organoids was shown in the statistical chart. At least 3 independent experiments were conducted. Results were shown as mean ± SD. ns, non-significant; $^{*}P < 0.05$, $^{*}P < 0.01$, $^{***}P < 0.001$.

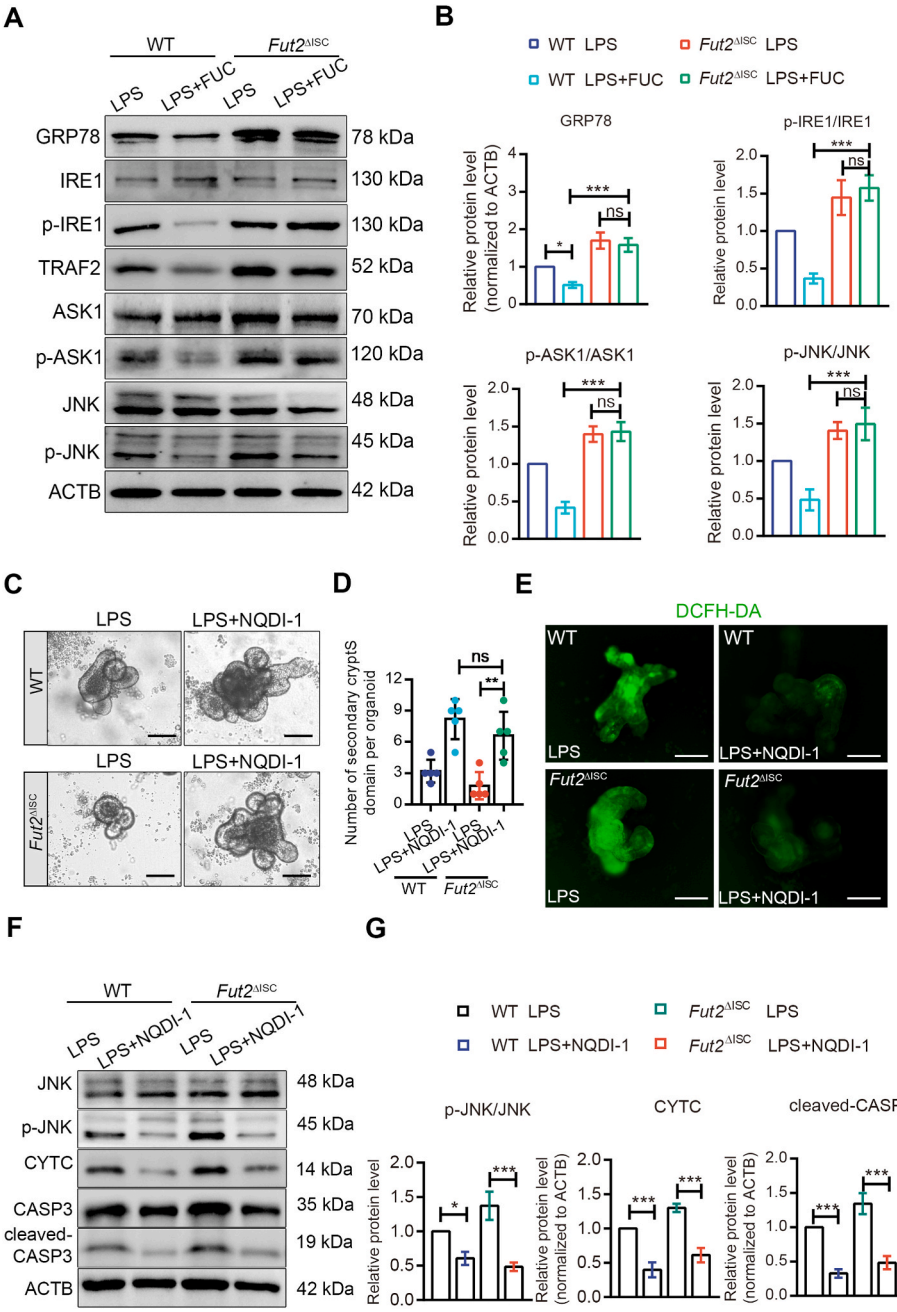

Fig. 8. Exacerbation of IRE1-mediated pro-apoptotic UPR signaling in *Fut2*$^{\Delta ISC}$ intestinal organoids. (A) Western blot analysis of UPR-related proteins in WT and *Fut2*$^{\Delta ISC}$ intestinal organoids. (B) Densitometric analysis of GRP78 and IRE1 signaling-related proteins in organoids was shown in the statistical chart. (C) Representative images of WT and *Fut2*$^{\Delta ISC}$ intestinal organoids exposed to LPS and NQDI-1. Scale bar: 50 μm. (D) Quantification and statistical analysis of the organoid buddings. (E) The ROS staining of intestinal organoids treated with LPS and NQDI-1 was detected by the DCFH-DA probe. Scale bar: 50 μm. (F) Western blot analysis of JNK, *p*-JNK, CYTC, and cleaved-CASP3 proteins in WT and *Fut2*$^{\Delta ISC}$ intestinal organoids treated with LPS and NQDI-1. (G) Densitometric analysis of *p*-JNK/JNK, CYTC, and cleaved-CASP3 in organoids was shown in the statistical chart. At least 3 independent experiments were conducted. Results were shown as mean ± SD. ns, non-significant; $^{*}P < 0.05$, $^{*}P < 0.01$, $^{***}P < 0.001$.

expression of γH2AX, a sensitive indicator of DNA damage, in GFP-labeled ISCs was significantly higher in the N862Q group than in the HYOU1 group, indicating that ISCs with aberrant fucosylation of HYOU1 were more sensitive to inflammatory injury (Fig. 10C). More specifically, N862Q showed a lower intensity of EdU signaling than the HYOU1 group in the LPS + FUC treated organoids ($P < 0.001$; Fig. 10D). The expression of *Lgr5* and *Olfm4* was also decreased in the N862Q group (Fig. 10E), indicating the stemness loss in the absence of correct fucosylation of HYOU1. Besides, N862Q exhibited diminished red fluorescent JC-1 aggregates and a lower red/green ratio, which reflected the MMP disruption and the mitochondrial dysfunction (Fig. 10F). Therefore, fucosylation defects in HYOU1 led to impaired self-renewal capacity and increased apoptosis in ISCs when exposed to inflammatory stimuli. Further, we examined the influence of HYOU1 fucosylation on triggering UPR signaling. The deficiency of HYOU1 fucosylation blocked the function of unfolded protein recognition and triggered the

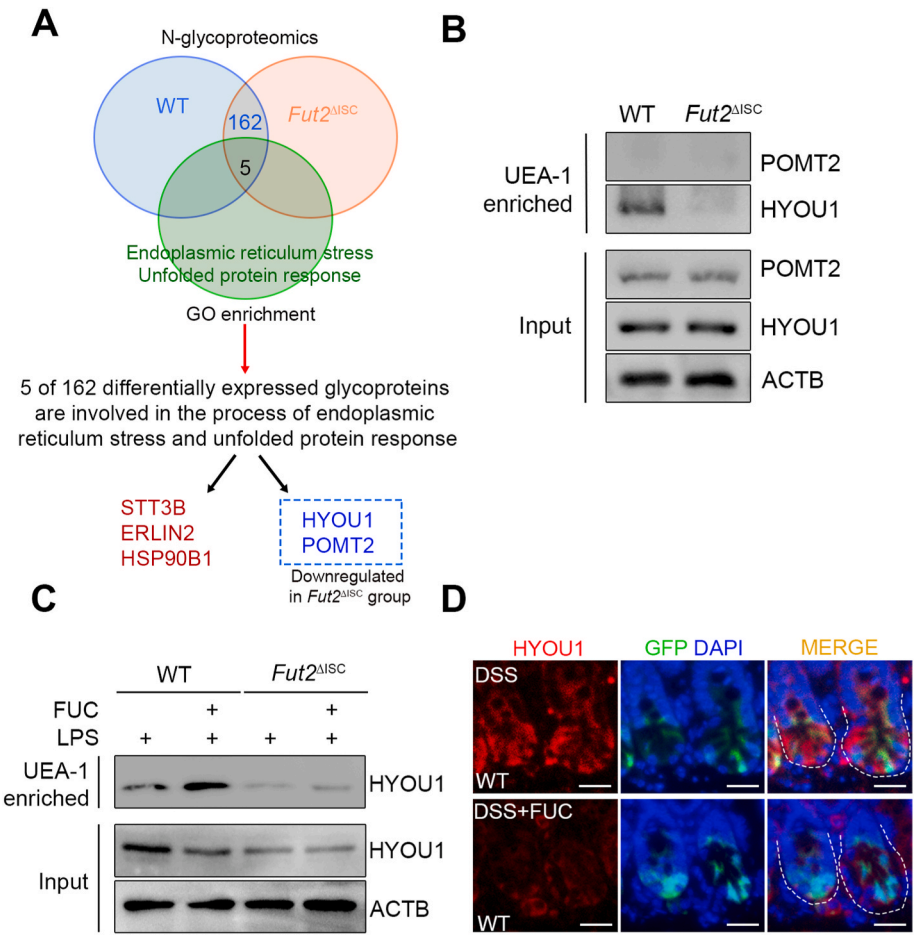

Fig. 9. Fucosylation of HYOU1 mediated by FUT2 in the process of unfolded protein response. (A) Venn diagram showed the number of proteins identified by *N*-glycoproteomics of ISCs from WT or *Fut2*$^{\Delta ISC}$ mice, as well as the proteins belonging to GO enrichment terms of ER stress and UPR. Five proteins were at the intersection among them. Two of the downregulated proteins in the *Fut2*$^{\Delta ISC}$ group were candidates for differential fucosylated molecules. (B) UEA-1 affinity chromatography of whole-cell lysates of intestinal organoids from WT and *Fut2*$^{\Delta ISC}$ mice, followed by Western blot with POMT2 and HYOU1 antibodies. (C) UEA-1 affinity chromatography of whole-cell lysates of WT and *Fut2*$^{\Delta ISC}$ intestinal organoids with the treatment of LPS and fucose, followed by Western blot with HYOU1 antibody. (D) Immunofluorescence staining of HYOU1 in intestine sections. ISCs were labeled with GFP antibody. Scale bar: 10 μm.

upregulation of GRP78 in the presence of fucose under LPS stimulation. Meanwhile, N862Q activated the phosphorylation of IRE1, ASK1, and JNK, leading to higher sensitivity to ER stress and aggravated cell apoptosis (Fig. 10G and H). Collectively, these results identified that fucosylation at the site of N862 of HYOU1 was essential for the recognition of unfolded proteins and the assistance with GRP78 in ER. As the crucial ER chaperone protein, fucosylated HYOU1 would hinder the activation of IRE1 and counteract excessive ER stress-induced oxidative stress and apoptosis, which in turn restored normal UPR states and cellular homeostasis in ISCs, and ultimately promoted epithelial repair and regeneration.

4. Discussion

In summary, our findings excavated the critical role of FUT2 as a regulator of ISCs and shed light on the complex question of how FUT2 affected the repair of the damaged intestinal epithelium. Here, we confirmed that fucose facilitated epithelial repair relying on the FUT2-dependent fucosylation of ISCs. In particular, fucose was proven to affect the survival and functions of ISCs upon inflammatory injury both *in vivo* and *ex vivo*. Mechanistically, in response to epithelial injury or aberrant fucosylation caused by FUT2 depletion, ER stress was triggered and then initiated UPR, of which the pro-apoptotic IRE1/TRAF2/ASK1/JNK signaling branch was activated. Of note, fucosylated HYOU1 at the site of Asn862 mediated by FUT2 suppressed the detrimental UPR branch and promoted ISCs resistance to detrimental stimuli.

In our study, we focused the effects of fucose on direct fucosylation of ISCs. Based on the previous study of our group which reported the decreased α-1,2-fucosylation in the intestine tissue of IBD patients and DSS-treated mice [31], we further revealed the diminished α-1,2-fucosylation in ISCs after injury both *in vivo* and *ex vivo*. On the basis of previous studies preliminarily elucidating the association between fucosylation deficiency and chronic colitis [30,32], we explored in depth the way fucosylation works. Fucose could restore the damaged state of ISCs by facilitating self-renewal and giving rise to differentiated cells to replenish the defective epithelium. In general, fucose provoked a rapid and extensive response to intestinal injury. In view of the limited efficacy and the increased risk of infections and cancer of immunosuppressive therapy for intestinal mucosal injury [39], the goal of achieving mucosal healing targeting ISCs supplemented with the natural monosaccharide is attractive. This finding may also collaboratively evidence the favorable role of fucose for the ingredients of exclusive enteral nutrition as earlier reported [27].

Impaired epithelial regeneration is closely related to deficient fucosylation. In this work, fucose failed to increase the number of organoid buds in the absence of FUT2, indicating the requirements of FUT2 for the self-renewal potential of ISCs. In practice, the self-renewal capacity governs stem cell-based regeneration to replenish the injured epithelium. Thus, FUT2-dependent fucosylation is identified as a protective mechanism that restores the homeostasis of ISCs via fine-tuning the dynamic balance between proliferation and differentiation. Moreover, FUT2 deficiency exacerbated MMP loss and terminally cell apoptosis, which in further support the necessity of FUT2 in preserving the number of ISCs. Mitochondrial function is deemed as the gatekeeper determining the fate of ISCs, which takes control of cellular metabolism, stress responses, and apoptosis [16,40]. Therefore, the disruption of MMP in intestinal organoids caused mitochondrial dysfunction, which in turn restrained the biosynthesis of amino acids, nucleotides, and lipids required for proliferating cells [41]. In this case, comprehensively understanding stem cells adaptations that maintain ISC homeostasis during

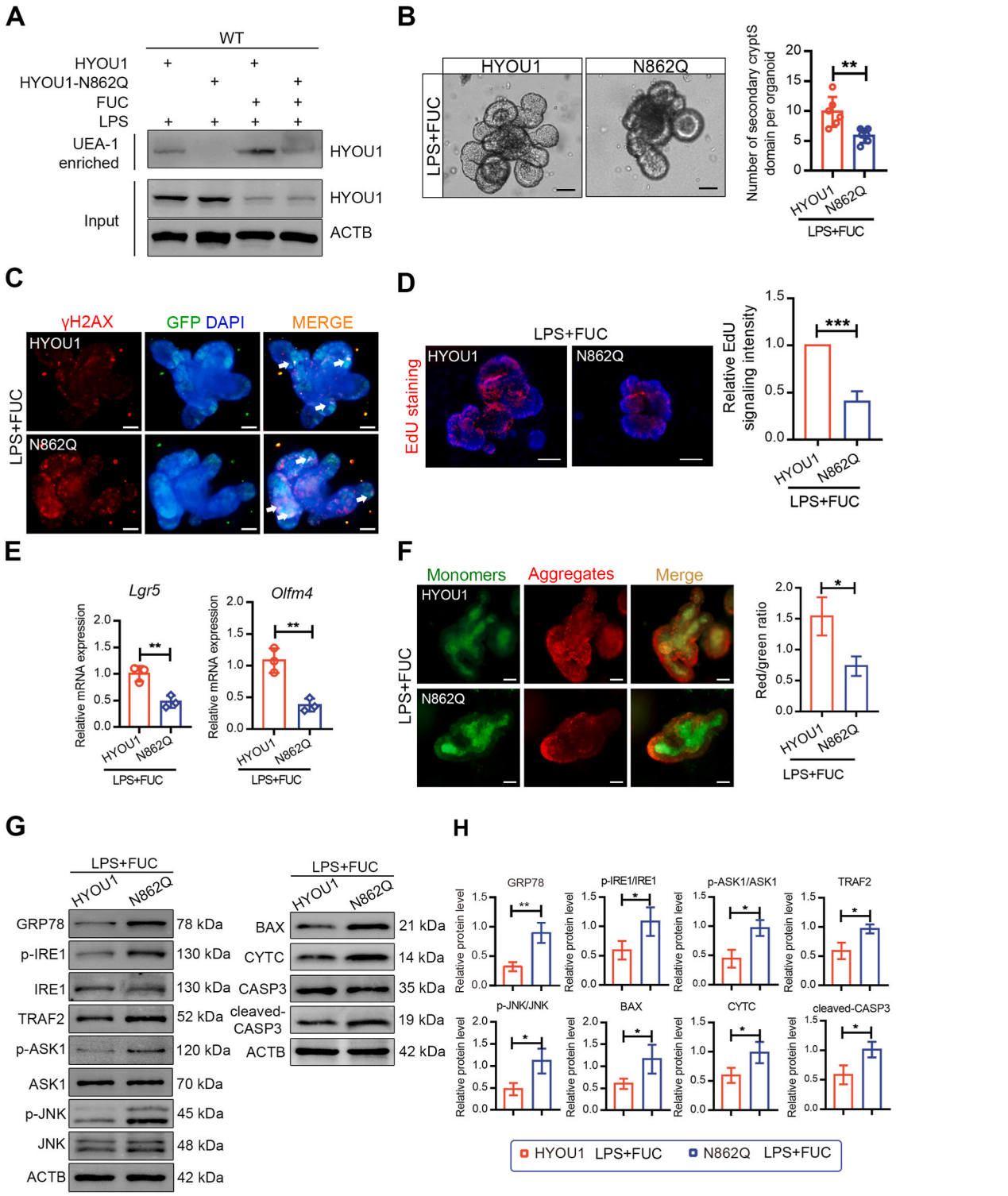

Fig. 10. Enhanced resistance to ER stress and injury in intestinal stem cells by fucosylation of HYOU1. (A) UEA-1 affinity chromatography of whole-cell lysates of HYOU1 (wild type) and N862Q (mutant for glycosylated HYOU1 modification site) intestinal organoids with the treatment of LPS and LPS + FUC, followed by Western blot with HYOU1 antibody. (B) Representative images of HYOU1 and N862Q intestinal organoids from WT mice exposed to LPS and LPS + FUC. Scale bar: 50 μm. Quantification analysis of the organoid buddings was shown in the right statistical chart. (C) Immunofluorescence staining of γH2AX in the HYOU1 and N862Q intestine organoids. The positive staining cells were indicated by white arrowheads. ISCs were labeled with GFP antibody. Scale bar: 50 μm. (D) EdU staining of HYOU1 and N862Q intestinal organoids from WT mice treated with LPS + FUC. Scale bar: 100 μm. The relative EdU signaling intensity (normalized to the HYOU1 group) was analyzed in the right statistical chart. (E) The mRNA expression level of stem cell markers *Lgr5* and *Olfm4*. (F) The JC-1 probe staining of HYOU1 and N862Q intestinal organoids was treated with LPS and FUC. Scale bar: 50 μm. Quantitative analysis of the red/green ratio was shown in the right statistical chart. (G) Western blot analysis of UPR- and apoptosis-related proteins in the HYOU1 and N862Q intestinal organoids. (H) Densitometric analysis of UPR-related and apoptosis-related proteins was shown in the right statistical chart. The relative protein level was normalized to the LPS + FUC treated HYOU1 group. At least 3 independent experiments were conducted. Results were shown as mean ± SD. $^{*}P < 0.05$, $^{*}P < 0.01$, $^{***}P < 0.001$. (For interpretation of the references to colour in this figure legend, the reader is referred to the Web version of this article.)

injury-induced intestinal regeneration is therefore a critical focus for stem cell biology [9].

To maintain homeostasis, the balance between ISC self-renewal and differentiation must be tightly balanced [42]. In the face of various microenvironments, different stem cell fate specifications, including self-renewal and differentiation, will be initiated and adapted to the actual cellular demand. ISCs remodel intestinal composition in response to epithelial defects by dividing symmetrically, either forming two daughter stem cells or two daughter non-stem progenitor cells which differentiate into the diverse types of epithelial cells [34,42]. A recent study has also revealed that ISC proliferation and differentiation are coordinately regulated to maintain homeostasis by regulating distinct pathways [43], which keeps in line with our results that FUT2-dependent fucosylation motivates the regenerative capacity of ISCs upon inflammatory injury.

Inflammatory stimuli are always regarded as the crucial elements for the perturbation of ER homeostasis and provoked ER stress, especially in the pathogenesis of mucosal injury disorders [15,44]. In the damaged epithelium, ISCs are particularly sensitive to ER stress [45]. On the other hand, the dysregulation of α-1,2-fucosylation, a class of *N*-glycosylation that mainly occurs in the ER, could result in the accumulation of misfolded or unfolded proteins and initiate UPR [19]. Thus, we proposed these two elements concurrently contributed to the activation of UPR deciphering the role of FUT2 in ISCs. Studies have shown that UPR coordinates stemness and cell fate under ER stress [16,46], and PERK knockdown or eIF2α dephosphorylation rescues the loss of stem cell markers and the translation of c-MYC, which is critical to maintain expression of a core set of Wnt target genes [20]. In this study, the constant stimulation of LPS triggered the activation of the pro-apoptotic branch of IRE1 sensor rather than PERK or ATF6, although the two sensors have also been reported to be associated with stemness loss [47]. This evidence demonstrated the precise control of UPR branches in stem cell fate determination. In this work, sustained IRE1 activity may serve as an activation platform for binding TRAF2, activating ASK1 and its downstream target JNK [48], which ultimately delivered signals to mitochondria and converged on the intrinsic apoptotic pathway. Unexpectedly, XBP1s, which was also activated by IRE1 and mediated ER associated degradation, was not restored by fucose. Similarly, the pro-oxidant *Txnip* was not altered by fucose, implying little correlation between caspase-1-dependent death with FUT2.

To gain insight into the mechanisms by which fucose promotes intestinal regeneration, *N*-glycoproteomics combined with UEA-1 chromatography identified fucosylated HYOU1, a major endoplasmic reticulum chaperone which coordinated pro-survival and stemness maintenance effects of FUT2 in ISCs. Similar to the well-known GRP78, HYOU1, a member of the HSP70 family that is responsible for protein import, guiding polypeptide folding, assembly of protein complexes, and channeling misfolded polypeptides to degradation [49], was upregulated in response to LPS or DSS stimuli both in intestinal tissue and organoids. In the presence of FUT2, we found that HYOU1 could effectively respond to inflammatory stimuli, and similar effects of HYOU1 have been detected in atherosclerosis and diabetic nephropathy [50,51]. Enhanced fucosylation of HYOU1 hindered the activation of pro-apoptotic UPR branch sensor IRE1, thereby mediating the adaptive UPR and inhibiting oxidative stress and apoptosis of ISCs. However, FUT2 depletion in ISCs invalidated the response of HYOU1 to inflammatory stimulation. Moreover, deficient HYOU1 fucosylation cannot actively block the progression of pro-apoptotic UPR signaling. Further validation for the α-1,2-fucosylation site of HYOU1 was conducted by generating a glycosylation-deficient mutant (N862Q) based on the data of *N*-glycoproteomics. Our results showed that N862Q substitution re-activated the IRE1/TRAF2/ASK1/JNK signaling, restrained the growth of intestinal organoids, exacerbated stemness loss and MMP disruption, and eventually led to apoptosis. Notably, the critical role of fucosylation on HYOU1 in regulating UPR initiation and stem cell fate was revealed for the first time. Meanwhile, HYOU1 serves as a nucleotide exchange factor (NEF) to regulate the canonical ER-localized HSP70 or GRP78 [52,53]. Besides, the fucosylated site of Asn862 may participate in forming a polar pocket connecting with the adenosine part of the ADP molecule to regulate the structure of GRP78 [38], and assist GRP78 binding to misfolded proteins to release the UPR sensors in response to ER stress [54]. Collectively, fucosylated HYOU1 constructed the bridge connecting FUT2 and UPR sensor IRE1. Therefore, our study identified a novel regulatory mechanism of UPR initiation by the fucosylated level of HYOU1.

5. Conclusion

In conclusion, FUT2 promotes survival and self-renewal of ISCs upon intestinal injury via regulating UPR and the fucosylated modification of the ER chaperone protein HYOU1. These findings not only emphasize the crucial role of FUT2-dependent fucosylation in the functions and survival of ISCs, but also highlight its involvement in the regulation of UPR and ER homeostasis, providing an appealing stem cell-based therapeutic approach for intestinal mucosal injury disorders.

Funding

This study was supported in part by the National Natural Science Foundation of China (No. 81974062, 82170570).

Author contributions

ZW, CT, and CH conceived and designed the study, ZW and CT conducted the experiment, ZW, CD, and JW performed data analysis, DZ, LH, WQ helped data analysis and interpretation, ZW drafted the article, CH and XH revised and approved the manuscript. All authors read and approved the final manuscript.

Declarations of competing interest

None.

Data availability

Data will be made available on request.

Acknowledgements

I would like to thank Yan Wang from The Institute of Hydrobiology, Chinese Academy of Sciences for the help with FACS.

Appendix A. Supplementary data

Supplementary data to this article can be found online at https://doi.org/10.1016/j.redox.2023.102618.

References

[1] E.C. Martens, M. Neumann, M.S. Desai, Interactions of commensal and pathogenic microorganisms with the intestinal mucosal barrier, Nat. Rev. Microbiol. 16 (8) (2018) 457–470.
[2] A. Albillos, A. de Gottardi, M. Rescigno, The gut-liver axis in liver disease: pathophysiological basis for therapy, J. Hepatol. 72 (3) (2020) 558–577.
[3] W. Choi, S. Yeruva, J.R. Turner, Contributions of intestinal epithelial barriers to health and disease, Exp. Cell Res. 358 (1) (2017) 71–77.
[4] D. Ma, P. Jiang, Y. Jiang, H. Li, D. Zhang, Effects of lipid peroxidation-mediated ferroptosis on severe acute pancreatitis-induced intestinal barrier injury and bacterial translocation, Oxid. Med. Cell. Longev. 2021 (2021), 6644576.
[5] K. Papamichael, W. Afif, D. Drobne, M.C. Dubinsky, M. Ferrante, P.M. Irving, N. Kamperidis, T. Kobayashi, P.G. Kotze, J. Lambert, N.M. Noor, X. Roblin, G. Roda, N. Vande Casteele, A.J. Yarur, N. Arebi, S. Danese, S. Paul, W.J. Sandborn, S. Vermeire, A.S. Cheifetz, L. Peyrin-Biroulet, M. International Consortium for Therapeutic Drug, Therapeutic drug monitoring of biologics in inflammatory bowel disease: unmet needs and future perspectives, Lancet. Gastroenterol. Hepatol 7 (2) (2022) 171–185.

[6] F. Deng, Z. Wu, F. Zou, S. Wang, X. Wang, The hippo-YAP/TAZ signaling pathway in intestinal self-renewal and regeneration after injury, Front. Cell Dev. Biol. 10 (2022), 894737.

[7] M.F. Neurath, S.P. Travis, Mucosal healing in inflammatory bowel diseases: a systematic review, Gut 61 (11) (2012) 1619–1635.

[8] C.Y. Liu, C.M. Cham, E.B. Chang, Epithelial wound healing in inflammatory bowel diseases: the next therapeutic frontier, Transl. Res. 236 (2021) 35–51.

[9] A.J.M. Santos, Y.H. Lo, A.T. Mah, C.J. Kuo, The intestinal stem cell niche: homeostasis and adaptations, Trends Cell Biol. 28 (12) (2018) 1062–1078.

[10] H.J. Snippert, L.G. van der Flier, T. Sato, J.H. van Es, M. van den Born, C. Kroon-Veenboer, N. Barker, A.M. Klein, J. van Rheenen, B.D. Simons, H. Clevers, Intestinal crypt homeostasis results from neutral competition between symmetrically dividing Lgr5 stem cells, Cell 143 (1) (2010) 134–144.

[11] A. Amcheslavsky, J. Jiang, Y.T. Ip, Tissue damage-induced intestinal stem cell division in Drosophila, Cell Stem Cell 4 (1) (2009) 49–61.

[12] C. Trentesaux, M. Fraudeau, C.L. Pitasi, J. Lemarchand, S. Jacques, A. Duche, F. Letourneur, E. Naser, K. Bailly, A. Schmitt, C. Perret, B. Romagnolo, Essential role for autophagy protein ATG7 in the maintenance of intestinal stem cell integrity, Proc. Natl. Acad. Sci. U. S. A. 117 (20) (2020) 11136–11146.

[13] G. Sorrentino, A. Perino, E. Yildiz, G. El Alam, M. Bou Sleiman, A. Gioiello, R. Pellicciari, K. Schoonjans, Bile acids signal via TGR5 to activate intestinal stem cells and epithelial regeneration, Gastroenterology 159 (3) (2020) 956–968 e8.

[14] E. Berger, E. Rath, D. Yuan, N. Waldschmitt, S. Khaloian, M. Allgauer, O. Staszewski, E.M. Lobner, T. Schottl, P. Giesbertz, O.I. Coleman, M. Prinz, A. Weber, M. Gerhard, M. Klingenspor, K.P. Janssen, M. Heikenwalder, D. Haller, Mitochondrial function controls intestinal epithelial stemness and proliferation, Nat. Commun. 7 (2016), 13171.

[15] S.S. Cao, E.M. Zimmermann, B.M. Chuang, B. Song, A. Nwokoye, J.E. Wilkinson, K. A. Eaton, R.J. Kaufman, The unfolded protein response and chemical chaperones reduce protein misfolding and colitis in mice, Gastroenterology 144 (5) (2013) 989–1000 e6.

[16] E. Rath, A. Moschetta, D. Haller, Mitochondrial function - gatekeeper of intestinal epithelial cell homeostasis, Nat. Rev. Gastroenterol. Hepatol. 15 (8) (2018) 497–516.

[17] A. Larabi, N. Barnich, H.T.T. Nguyen, New insights into the interplay between autophagy, gut microbiota and inflammatory responses in IBD, Autophagy 16 (1) (2020) 38–51.

[18] R.E. Sanchez-Pupo, D. Johnston, S. Penuela, N-glycosylation regulates pannexin 2 localization but is not required for interacting with pannexin 1, Int. J. Mol. Sci. 19 (7) (2018).

[19] C. Hetz, F.R. Papa, The unfolded protein response and cell fate control, Mol. Cell 69 (2) (2018) 169–181.

[20] J. Heijmans, J.F. van Lidth de Jeude, B.K. Koo, S.L. Rosekrans, M.C. Wielenga, M. van de Wetering, M. Ferrante, A.S. Lee, J.J. Onderwater, J.C. Paton, A.W. Paton, A.M. Mommaas, L.L. Kodach, J.C. Hardwick, D.W. Hommes, H. Clevers, V. Muncan, G.R. van den Brink, ER stress causes rapid loss of intestinal epithelial stemness through activation of the unfolded protein response, Cell Rep. 3 (4) (2013) 1128–1139.

[21] S.L. Rosekrans, J. Heijmans, N.V. Buller, J. Westerlund, A.S. Lee, V. Muncan, G. R. van den Brink, ER stress induces epithelial differentiation in the mouse oesophagus, Gut 64 (2) (2015) 195–202.

[22] E.G. Foerster, T. Mukherjee, L. Cabral-Fernandes, J.D.B. Rocha, S.E. Girardin, D. J. Philpott, How autophagy controls the intestinal epithelial barrier, Autophagy 18 (1) (2022) 86–103.

[23] I.M. Ibrahim, D.H. Abdelmalek, A.A. Elfiky, GRP78: a cell's response to stress, Life Sci. 226 (2019) 156–163.

[24] G.S. Hotamisligil, Endoplasmic reticulum stress and the inflammatory basis of metabolic disease, Cell 140 (6) (2010) 900–917.

[25] K. Zhang, R.J. Kaufman, From endoplasmic-reticulum stress to the inflammatory response, Nature 454 (7203) (2008) 455–462.

[26] R. He, Y. Li, C. Han, R. Lin, W. Qian, X. Hou, L-Fucose ameliorates DSS-induced acute colitis via inhibiting macrophage M1 polarization and inhibiting NLRP3 inflammasome and NF-kB activation, Int. Immunopharm. 73 (2019) 379–388.

[27] Y. Li, Y. Jiang, L. Zhang, W. Qian, X. Hou, R. Lin, Exogenous l-fucose protects the intestinal mucosal barrier depending on upregulation of FUT2-mediated fucosylation of intestinal epithelial cells, Faseb. J. 35 (7) (2021), e21699.

[28] M. Viladomiu, M.L. Metz, S.F. Lima, W.B. Jin, L. Chou, J.R.I.L.C. Bank, C.J. Guo, G. E. Diehl, K.W. Simpson, E.J. Scherl, R.S. Longman, Adherent-invasive E. coli metabolism of propanediol in Crohn's disease regulates phagocytes to drive intestinal inflammation, Cell Host Microbe 29 (4) (2021) 607–619 e8.

[29] Y. Goto, T. Obata, J. Kunisawa, S. Sato, Ivanov II, A. Lamichhane, N. Takeyama, M. Kamioka, M. Sakamoto, T. Matsuki, H. Setoyama, A. Imaoka, S. Uematsu, S. Akira, S.E. Domino, P. Kulig, B. Becher, J.C. Renauld, C. Sasakawa, Y. Umesaki, Y. Benno, H. Kiyono, Innate lymphoid cells regulate intestinal epithelial cell glycosylation, Science 345 (6202) (2014), 1254009.

[30] Y. Goto, S. Uematsu, H. Kiyono, Epithelial glycosylation in gut homeostasis and inflammation, Nat. Immunol. 17 (11) (2016) 1244–1251.

[31] X. Tang, W. Wang, G. Hong, C. Duan, S. Zhu, Y. Tian, C. Han, W. Qian, R. Lin, X. Hou, Gut microbiota-mediated lysophosphatidylcholine generation promotes colitis in intestinal epithelium-specific Fut2 deficiency, J. Biomed. Sci. 28 (1) (2021) 20.

[32] Y. Wang, D. Huang, K.Y. Chen, M. Cui, W. Wang, X. Huang, A. Awadellah, Q. Li, A. Friedman, W.W. Xin, L. Di Martino, F. Cominelli, A. Miron, R. Chan, J.G. Fox, Y. Xu, X. Shen, M.F. Kalady, S. Markowitz, I. Maillard, J.B. Lowe, W. Xin, L. Zhou, Fucosylation deficiency in mice leads to colitis and adenocarcinoma, Gastroenterology 152 (1) (2017) 193–205 e10.

[33] H.S. Cooper, S.N. Murthy, R.S. Shah, D.J. Sedergran, Clinicopathologic study of dextran sulfate sodium experimental murine colitis, Lab. Invest. 69 (2) (1993) 238–249.

[34] S. Beyaz, M.D. Mana, J. Roper, D. Kedrin, A. Saadatpour, S.J. Hong, K.E. Bauer-Rowe, M.E. Xifaras, A. Akkad, E. Arias, L. Pinello, Y. Katz, S. Shinagare, M. Abu-Remaileh, M.M. Mihaylova, D.W. Lamming, R. Dogum, G. Guo, G.W. Bell, M. Selig, G.P. Nielsen, N. Gupta, C.R. Ferrone, V. Deshpande, G.C. Yuan, S.H. Orkin, D. M. Sabatini, O.H. Yilmaz, High-fat diet enhances stemness and tumorigenicity of intestinal progenitors, Nature 531 (7592) (2016) 53–58.

[35] J.H. Loong, T.L. Wong, M. Tong, R. Sharma, L. Zhou, K.Y. Ng, H.J. Yu, C.H. Li, K. Man, C.M. Lo, X.Y. Guan, T.K. Lee, J.P. Yun, S.K. Ma, Glucose deprivation-induced aberrant FUT1-mediated fucosylation drives cancer stemness in hepatocellular carcinoma, J. Clin. Invest. 131 (11) (2021).

[36] J. Drost, R.H. van Jaarsveld, B. Ponsioen, C. Zimberlin, R. van Boxtel, A. Buijs, N. Sachs, R.M. Overmeer, G.J. Offerhaus, H. Begthel, J. Korving, M. van de Wetering, G. Schwank, M. Logtenberg, E. Cuppen, H.J. Snippert, J.P. Medema, G. J. Kops, H. Clevers, Sequential cancer mutations in cultured human intestinal stem cells, Nature 521 (7550) (2015) 43–47.

[37] T. Sato, R.G. Vries, H.J. Snippert, M. van de Wetering, N. Barker, D.E. Stange, J. H. van Es, A. Abo, P. Kujala, P.J. Peters, H. Clevers, Single Lgr5 stem cells build crypt-villus structures in vitro without a mesenchymal niche, Nature 459 (7244) (2009) 262–265.

[38] P.P. Pagare, H. Wang, X.Y. Wang, Y. Zhang, Understanding the role of glucose regulated protein 170 (GRP170) as a nucleotide exchange factor through molecular simulations, J. Mol. Graph. Model. 85 (2018) 160–170.

[39] E.J. Villablanca, K. Selin, C.R.H. Hedin, Mechanisms of mucosal healing: treating inflammatory bowel disease without immunosuppression? Nat. Rev. Gastroenterol. Hepatol. 19 (8) (2022) 493–507.

[40] E. Urbauer, E. Rath, D. Haller, Mitochondrial metabolism in the intestinal stem cell niche-sensing and signaling in health and disease, Front. Cell Dev. Biol. 8 (2020), 602814.

[41] J.C. Schell, D.R. Wisidagama, C. Bensard, H. Zhao, P. Wei, J. Tanner, A. Flores, J. Mohlman, L.K. Sorensen, C.S. Earl, K.A. Olson, R. Miao, T.C. Waller, D. Delker, P. Kanth, L. Jiang, R.J. DeBerardinis, M.P. Bronner, D.Y. Li, J.E. Cox, H. R. Christofk, W.E. Lowry, C.S. Thummel, J. Rutter, Control of intestinal stem cell function and proliferation by mitochondrial pyruvate metabolism, Nat. Cell Biol. 19 (9) (2017) 1027–1036.

[42] G. Huelsz-Prince, R.N.U. Kok, Y. Goos, L. Bruens, X. Zheng, S. Ellenbroek, J. Van Rheenen, S. Tans, J.S. van Zon, Mother cells control daughter cell proliferation in intestinal organoids to minimize proliferation fluctuations, Elife 11 (2022).

[43] J.H. Won, J.S. Choi, J.I. Jun, CCN1 interacts with integrins to regulate intestinal stem cell proliferation and differentiation, Nat. Commun. 13 (1) (2022) 3117.

[44] D. Qiao, Z. Zhang, Y. Zhang, Q. Chen, Y. Chen, Y. Tang, X. Sun, Z. Tang, Y. Dai, Regulation of endoplasmic reticulum stress-autophagy: a potential therapeutic target for ulcerative colitis, Front. Pharmacol. 12 (2021), 697360.

[45] B.J. Meijer, W.L. Smit, P.J. Koelink, B.F. Westendorp, R.J. de Boer, J.H.M. van der Meer, J.L.M. Vermeulen, J.C. Paton, A.W. Paton, J. Qin, E. Dekker, V. Muncan, G. R. van den Brink, J. Heijmans, Endoplasmic reticulum stress regulates the intestinal stem cell state through CtBP2, Sci. Rep. 11 (1) (2021) 9892.

[46] Z. Zhang, L. Zhang, L. Zhou, Y. Lei, Y. Zhang, C. Huang, Redox signaling and unfolded protein response coordinate cell fate decisions under ER stress, Redox Biol. 25 (2019), 101047.

[47] C.N. Spaan, W.L. Smit, J.F. van Lidth de Jeude, B.J. Meijer, V. Muncan, G.R. van den Brink, J. Heijmans, Expression of UPR effector proteins ATF6 and XBP1 reduce colorectal cancer cell proliferation and stemness by activating PERK signaling, Cell Death Dis. 10 (7) (2019) 490.

[48] K. Castillo, D. Rojas-Rivera, F. Lisbona, B. Caballero, M. Nassif, F.A. Court, S. Schuck, C. Ibar, P. Walter, J. Sierralta, A. Glavic, C. Hetz, BAX inhibitor-1 regulates autophagy by controlling the IRE1alpha branch of the unfolded protein response, EMBO J. 40 (21) (2021), e109149.

[49] J. Behnke, M.J. Feige, L.M. Hendershot, BiP and its nucleotide exchange factors Grp170 and Sil 1: mechanisms of action and biological functions, J. Mol. Biol. 427 (7) (2015) 1589–1608.

[50] M.T. Lindenmeyer, M.P. Rastaldi, M. Ikehata, M.A. Neusser, M. Kretzler, C. D. Cohen, D. Schlondorff, Proteinuria and hyperglycemia induce endoplasmic reticulum stress, J. Am. Soc. Nephrol. 19 (11) (2008) 2225–2236.

[51] M. Sanson, C. Ingueneau, C. Vindis, J.C. Thiers, Y. Glock, H. Rousseau, Y. Sawa, Y. Bando, Z. Mallat, R. Salvayre, A. Negre-Salvayre, Oxygen-regulated protein-150 prevents calcium homeostasis deregulation and apoptosis induced by oxidized LDL in vascular cells, Cell Death Differ. 15 (8) (2008) 1255–1265.

[52] T.M. Buck, L. Plavchak, A. Roy, B.F. Donnelly, O.B. Kashlan, T.R. Kleyman, A. R. Subramanya, J.L. Brodsky, The Lhs1/GRP170 chaperones facilitate the endoplasmic reticulum-associated degradation of the epithelial sodium channel, J. Biol. Chem. 288 (25) (2013) 18366–18380.

[53] T. Inoue, B. Tsai, The Grp170 nucleotide exchange factor executes a key role during ERAD of cellular misfolded clients, Mol. Biol. Cell 27 (10) (2016) 1650–1662.

[54] S. Preissler, D. Ron, Early events in the endoplasmic reticulum unfolded protein response, Cold Spring Harbor Perspect. Biol. 11 (4) (2019).